Optimized Phosphors for Warm White LED Light Engines
(DE-EE-0003251)
Final Report

Performer:
GE Global Research
Other Team Members:
GE Lighting Solutions LLC (GELS), East Cleveland, OH
University of Georgia (UGA), Athens, GA

Principal Investigator
Anant Setlur
GE Global Research
1 Research Circle, Room K1-4A17
Niskayuna, NY 12309
(518)387-6305
setlur@ge.com

Program Team:
GE Global Research
Megan Brewster
Florencio Garcia
M. Christine Hill
Robert Lyons
James Murphy
Tom Stecher
Stan Stoklosa
Stan Weaver
University of Georgia
Prof. Uwe Happek
GE Lighting Solutions
Danny Aesram
Anirudha Deshpande

Executive summary:

The objective of this program is to develop phosphor systems and LED light engines that have steady-state LED efficacies (using LEDs with a 60% wall-plug efficiency) of 105–120 lm/W with correlated color temperatures (CCT) ~3000 K, color rendering indices (CRI) >85, <0.003 distance from the blackbody curve (dbb), and <2% loss in phosphor efficiency under high temperature, high humidity conditions. In order to reach these goals, this involves the composition and processing optimization of phosphors previously developed by GE in combination with light engine package modification. To meet these requirements, the accomplishments of this program have been:

- Development of optical models for remote phosphor systems with correlation to phosphor scattering and absorption coefficients derived from direct measurement of powder phosphors.
- Development of fundamental models for the thermal quenching of the green phosphors within this program. These models point to an inherent limit in the activator concentration which leads us to the conclusion that the reduction in scattering losses in these materials will come from particle size/morphology modifications, not compositional changes.
- Use of the combined optical and thermal model to set guidelines for phosphor properties (particle size distribution, parasitic absorption, etc.) and development paths for the phosphors in this program.
- Invention and development of particle coating chemistries to coat our $(Sr,Ca)_3(Al,Si)O_4(F,O):Ce^{3+}$ particles in order to prevent degradation under high temperature, high humidity (HTHH) conditions.
- Development of elutriation methods to remove fine particles that arise from phosphor milling and that disproportionally contribute to the scattering coefficient of our phosphors. In some cases, these methods can reduce the phosphor scattering coefficient by ~40% with <20% mass loss through the removal of fine particles.
- Scale-up and optimization at 50 g scale for all green phosphors; the quantum efficiency of our green phosphors ranges from 87-90% with batch-to-batch variability. We have also scaled-up our particle coating methods for moisture protection of our $(Sr,Ca)_3(Al,Si)O_4(F,O):Ce^{3+}$ green phosphor. Optimization of elutriation/decanting methods to remove fine particles that arise from phosphor milling and that disproportionally contribute to the scattering coefficient of our phosphors. Apart from the reduction in phosphor scattering coefficient, we have also found that the "fine" particles in our samples also have lower quantum efficiency. The removal of these fine particles has led to the high quantum efficiencies for all of our phosphors.
- Optimization of our $K_2SiF_6:Mn^{4+}$ (PFS) line-emitting phosphor to have quantum efficiencies of 83-87% while minimizing degradation under high temperature, high humidity (HTHH) conditions.
- Development of 40-800 lumen (pulsed) light engines that have phosphor/package efficiencies of ~185-225 lm/W_{blue} at 2800-4000K, CRI=90-95. **We believe that these values are higher than any other high CRI phosphor system currently used in LED lighting and have confirmed this through initial testing versus commercial remote phosphor parts.** We initially prototyped these packages using LEDs with wall-plug efficiencies of 45-50% at 350 mA. Scaling this to our program goals with a 60% LED wall-plug efficiency gives a pulsed efficacy of 111-135 lm/W. We have confirmed this estimate by making lower drive current measurements at the NVLAB-accredited integrating spheres at GE Lighting.
- Development of quantitative relationships for steady-state losses in these remote phosphor systems with the single input of incident blue flux on the thermally isolated remote phosphor part. For incident fluxes of <0.25 W/cm^2, the phosphor temperatures are <75°C with a steady state loss of ~3-4%. At higher incident fluxes, phosphor temperatures can easily exceed 125°C with thermal losses at steady state of >10%. There are three primary loss paths for these thermal losses: LED heating (~3-4%), reduced phosphor absorption (~2%), and reduced phosphor quantum efficiency (~6-8%).
- Development of accelerated reliability tests and initial quantitative relationships for phosphor reliability versus incident blue light flux and phosphor temperature. We have found some limitations for the reliability of the current PFS line-emitting phosphor at very high fluxes

(>3 W/cm^2) and moderate temperatures (>85^{o}C). This places inherent limitations on system and LED package designs using this phosphor. However, in Vio^{TM}-like prototypes, we have made ~400 lm packages that have had <1% lumen loss and <1 MacAdam ellipse color shift over 4000 hours.

- Identification of an external toll vendor in Pennsylvania for one green phosphor composition and qualification of our optimized synthesis procedures at this toll vendor. Initial transition of PFS synthesis to an external toll vendor in Oklahoma, who has matched the quantum efficiency of our internal PFS samples at 50 g scale.

Program milestones & status:

Task 2:

Intermediate milestones

Title: Determine composition (i.e. activator concentration) vs. thermal quenching parameters & guidelines for concentration-based thermal quenching (6/15/2010)

Status: Characterized relative quantum efficiency from 25-200^{o}C for blue, green, orange, and red phosphors completed & developed fundamental model for high temperature quenching mechanisms.

Title: Measurements for optical constants (absorption coefficient, refractive index, scattering parameters) for current phosphor compositions (6/30/2010).

Status: Developed and verified methods to decouple absorption and scattering within powder phosphor. We are using measurement techniques to evaluate all phosphors in program. Also, determined that parasitic absorption is present in red-line emitting phosphors that need to be reduced/removed in order to optimize package efficiency.

Title: Initial optical model for remote phosphor packages & correlation with current GELS package performance under pulsed operation (8/15/2010)

Status: Developed two-flux model incorporating optical losses, scattering, phosphor quantum efficiency, and geometry of current Lumination packages that can predict package efficacy differences for both blue and violet LED packages. Used model to assign relative weights for package and phosphor modifications.

Title: Integrated optical & thermal models for remote phosphor package (9/15/2010)

Status: Developed fundamental understanding of thermal quenching in some of Ce^{3+}-phosphors (SASOF/YAG), need to integrate further into package models for steady-state performance. Developed methods to measure phosphor temperature *in situ* using the spectral parameters of the PFS red-line emitting phosphor.

Task 2 deliverable

Title: Design parameters for phosphor particle size and morphology combined with package design for 20% improvement in steady-state efficacy (9/30/2010)

Status: Package model has determined that 15-20% improvements are possible by increasing package reflectivity to ~90% with an additional 5-10% improvements are possible through reduction of phosphor scattering losses (@90% package reflectivity). Improvements from phosphor scattering will become larger at lower package reflectivities. Also, removal of

parasitic absorption in the red line emitter can also lead to >5% improvement in package efficiency.

Task 3:

Intermediate Milestones

Title: Demonstrate larger particle size blue phosphor with semi-infinite plaque absorption >75% (vs. ~55% currently) with no loss in QE (RT & 150C) & similar plaque reliability (8/31/2010)

Status: Increased particle size and Eu^{2+} concentration in blue phosphor without concentration quenching. Modified phosphor stoichiometry and excess halide levels (fluxing) to improve reliability in plaque testing. Materials sent to GELS for lamp testing. Further work stopped due to focus on blue LED-based systems.

Title: Develop synthesis and/or coating methods to protect current green & deep red phosphors from 85C/85%RH (HTHH) conditions; <5% loss after 100 hrs under direct HTHH exposure (10/15/2010)

Status: Developed numerous coating strategies for SASOF green phosphor that minimize moisture sensitivity. No losses in phosphor quantum efficiency; optimization gives thinner coatings that minimize scattering losses. Materials sent to GELS for lamp testing.

Title: Demonstrate classification method to remove fine particles for current green and orange phosphor particles; improve semi-infinite plaque absorption by >5% versus non-classified particles

Planned Date: 11/30/2010

Status: Developed elutriation methods to remove fine particles from powder phosphors. Reduced phosphor scattering coefficients by >40%, yielding increases in d_{10} particle size and semi-infinite plaque absorption of 7-10% depending upon phosphor composition. Adopted as best practice for all phosphors in this program.

Title: Demonstrate synthesis method to increase particle size in current orange phosphor particles to increase semi-infinite plaque absorption by 10%

Planned Date: 3/31/2011

Status: Developed fluxing system for orange phosphor to increase particle size and semi-infinite plaque absorption at lower activator concentrations. Current issue with fluxing system is reactivity with furnace components reducing component lifetime. Using initial knowledge to modify furnace or fluxing system. Work stopped to focus upon synthesis of red-line emitting phosphor in order to simultaneously improve CRI & lumen equivalent.

Title: Demonstrate synthesis method to narrow particle size distribution in current green phosphor particles to d10~>8 μm

Planned Date: 3/31/2011

Status: Initial testing within our silicate garnet phosphors has shown that modification of the initial stoichiometry of the materials leads to a lower d_{10} of ~8 μm and a significantly larger plaque absorption. Optical testing of modified garnets whose fine particles were removed by decanting/elutriation showed improve phosphor conversion efficiency by ~3-5%.

Title: Optimize synthesis method for larger particle size green/orange phosphor to match current RT QE (6/30/2011)
Status: For the silicate garnet phosphors, our optimized synthesis method was based upon non-stoichiometric starting compositions to minimize 2nd phase formation and Ce^{3+} segregation into these 2nd phases. For our red-line emitting phosphors, we optimized the phosphor synthesis through control over precipitation processes.

Title: Iterative optimization of particle size/composition based upon model in Task 2 & Task 4 results (9/30/2011)
Status: We have continued phosphor optimization to minimize parasitic absorptions in these phosphors, primarily through removal of parasitic 2nd phases. The primary focus has been on our red-line emitting phosphor and control over the pH during synthesis to minimize K_2MnF_6 decomposition that both reduces the amount of Mn^{4+} incorporated into the phosphor and also leads to a brown parasitic absorption.

Task 3 final deliverable:
Title: Demonstrate synthesis at 50-100 g batch scale for optimized composition & synthesis with QE>85% and meeting size distribution and morphology requirements defined from Task 2 (12/30/2011)
Status: We have demonstrated 50 g scale-up of all green phosphors including the moisture protective coating of the SASOF phosphor. We have worked with a toll vendor in Pennsylvania (outside of this program) and have made these phosphors at larger scales. In addition, we have transitioned the synthesis of our red line-emitting phosphor to an external toll vendor in Oklahoma, and our external toll vendor has matched the quantum efficiency of our internal 5-10 g samples at 50 g scale.

Task 4:
Title: Demonstrate 10% steady-state package efficiency improvement (currently 65% at steady state) improvement versus current 350 lumen prototypes (12/15/2010)
Status: Demonstrated lumen improvement in lower lumen packages using reflective insets instead of typical printed circuit boards. Package efficiency is currently at 70% versus 65% in prior systems. Assigned one loss to parasitic phosphor absorption in red-line emitter phosphor.

Title: Demonstrate 10% steady-state package efficiency (currently 65% at steady state) improvement versus current 700 lumen prototypes (3/30/2011)
Title: Demonstrate 20% steady-state package efficiency improvement versus current 350 lumen prototypes (9/30/2011)
Title: Demonstrate 20% steady-state package efficiency improvement versus current 700 lumen prototypes meeting reliability (<1% lumen loss and d(u,v) shift of 0.003 over 5000 hrs of room temperature operation) (3/30/2012)
Status: We have tested the efficacy of various phosphor geometries using a light engines using a board populated with 7 Cree royal blue LED packages. We have generally found that hemispherical phosphor domes have significant improvements in efficacy versus cylindrical light engines in accordance with our optical models. Consequently, we are able to reach efficiencies of 78-82% in flash measurements & 72-76% phosphor efficiencies in steady state measurements at 350 mA drive currents. We have taken these values higher in linear light engines with angled

side walls that have total efficiencies of ~85% with a phosphor/package efficiency of ~220 lm/W_{blue}. All of these values represent an improvement of >20% of our initial phosphor efficiency at the program start. In our current phosphors, we have found that there are both efficacy and reliability limitations when the steady-state phosphor temperature exceeds 80°C. Most of the reliability concerns come from the PFS red-line emitting phosphor, so we have also studied the reliability of this phosphor in greater detail. We also tested our phosphors for blue light damage under accelerated conditions using a blue laser. Taking the results from the accelerated damage experiments, we believe that our remote phosphor light engines should meet both lumen loss and color shift metrics for reliability, provided that the incident flux on the phosphor is <0.5 W/cm^2 with a phosphor temperature <80°C. We have initially validated these parameters through testing of PFS-based blends in Vio™-like prototypes and will be continuing reliability testing in various light engine configurations.

Detailed Technical Report

Project Objective:

GE Global Research, in collaboration with GELS and the University of Georgia (UGA), is executing a two-year program to develop optimized phosphor systems and light engine packaging for warm white LEDs. This program will build upon the materials and understanding developed in prior DOE programs between GE and UGA that have led to new phosphors and light engine prototypes with ~82 lm/W efficacy (pulsed) at CCT~3100 K, CRI~90, and R9~80. This program aims to increase the total efficiency for phosphor downconversion from ~70% towards the 90% phosphor efficiency that is typical for fluorescent lighting by reducing scattering and thermal losses in high quantum yield phosphor coatings. Program success will significantly improve the steady-state efficacy of warm white LED light engines, enabling steady-state LED efficacies (using LEDs with a 60% wall-plug efficiency) of 105–120 lm/W with correlated color temperatures (CCT) ~3000 K, color rendering indicies (CRI) >85, and <0.003 distance from the blackbody curve (dbb).

1. Technical Approach and Work Plan:

This program builds upon previous DOE-sponsored GE/UGA programs (DE-FC26-04NT41945 and DE-FC26-06NT42934) as well as internal GE programs to develop and optimize new phosphors materials. This work has helped to lead to the introduction of the Vio™ light engine and developed improved green, yellow, and orange phosphors with quantum efficiencies (in spectrometer measurements) of >85%. In addition, our internal GE programs have also developed unique red-line emitting phosphors that help to significantly reduce the efficacy gaps between high CRI, warm white lamps and cool white lamps[1] (Figure 1). These phosphors have been prototyped in high efficacy, warm white light engines using either blue or violet LEDs with:

- >25% higher efficacy at steady-state versus current Vio™ blends at ~3200 K, CRI=82 using 405 nm LEDs; pulsed and steady-state efficacies of 55 lm/W and 48 lm/W, respectively
- Pulsed efficacy of 82 lm/W at CCT~3000 K, CRI~90 lamps using 450 nm LEDs at ~270 lumens (Figure 1); steady state efficacies of 70 lm/W
- <1% loss in phosphor efficiency and no phosphor color shift for >5000 hrs of lamp testing for our green and orange phosphors

Since we have a relatively full portfolio of phosphors that are useful for both blue and violet LED excitation, our targeted improvements in phosphor downconversion from this program will be applicable regardless of InGaN LED wavelength. However, when accounting for both the reduced Stokes loss and the ability to use our red-line emitting phosphor to improve both lumen equivalent and color rendering, our focus in 2011 has been mainly towards blue LED-based systems.

[1] A.A. Setlur et al. Chem. Mater., **22**, 4076 (2010).

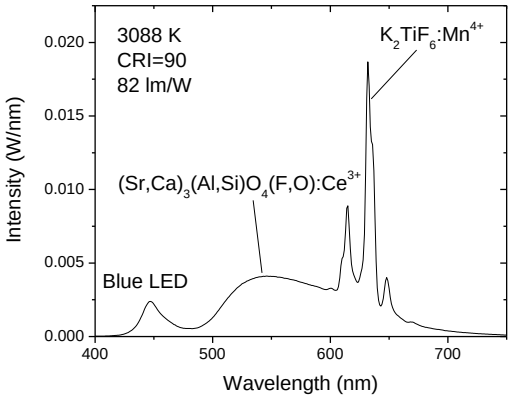

Figure 1. Spectral power distribution of lamp using blue LEDs, the SASOF green phosphor developed under DOE-sponsored work, and $K_2TiF_6:Mn^{4+}$, one of the GE red-line emitting phosphors[1].

The GE development efforts have led to efficient phosphors that can be used for LED lamps with different CCTs/CRIs/LED wavelengths, but significant progress is still necessary to improve the total phosphor conversion efficiency in LED lamps and packages (Table 1). For example, thicker phosphor coatings are needed in warm white packages, leading to additional losses from scattering into lossy packages and light engines. There are also significant thermal issues that affect or arise from phosphor downconversion. Phosphor downconversion leads to an increase in phosphor temperatures due to Stokes losses. This leads to additional phosphor quenching and additional heat generation in the phosphor layer until steady-state conditions are reached. Also, these higher phosphor temperatures will heat the LED board and chip, leading to LED wavelength shifts and light output losses from the LED thermal quenching. From our previous program, the LED board temperature in devices using our new phosphor blends that have higher quantum efficiencies at elevated temperatures leads to significantly lower board temperatures (>15°C) versus the phosphor blends in typical 6 chip Vio devices. The reduction in package temperature from switching phosphor blends can therefore lead to larger improvements in LED efficacy beyond just higher phosphor quantum efficiencies at elevated temperatures.

Table 1. Losses and efficacy in GE's LED prototype light engines

	LED WPE	Stokes loss	Lumen equivalent	Total phosphor conversion efficiency	Pulsed efficacy (350 mA)	Thermal losses (passive cooling)	Steady-state efficacy
Current Vio™ light engine	40%	72%	260 lm/W_{rad}	62%	46 lm/W	23%	35 lm/W
Current violet LED + phosphor light engine prototypes (CRI~80)	40%	72%	260 lm/W_{rad}	72%	55 lm/W	15%	47 lm/W
Current blue LED + phosphor light engine prototype (CRI~90)	43%	80%	325 lm/W_{rad}	72%	82 lm/W	15%	70 lm/W
Future LED light engines (CCT<3000 K, CRI>85)	60%	72% (violet) 80% (blue)	325 lm/W_{rad}	80%	110-125 lm/W	5%	105-120 lm/W

While scattering and thermal losses are significant in total, they represent the product of many smaller losses within LED light engines. Therefore, to achieve the program goals, there are three main tasks within this program:

1. Quantify the loss mechanisms when our new phosphors are incorporated into light engines using either blue or violet LEDs and correlate with optical and thermal models for phosphor downconversion in LED packages.
2. The output of these models will guide the composition and synthesis of our phosphors and the optimal light engine design. Meeting specific phosphor goals for size, morphology, and composition will use the team's experience in phosphor development and fundamental measurements of phosphor quenching.
3. Finally, these new phosphors will be integrated into LED light engines designed to maximize light engine efficacy. The results of this program will bring the phosphor conversion efficiency, including scattering losses, towards that of fluorescent lamps.

The high quantum efficiency of the phosphors within the GE portfolio narrows the program goal towards minimizing the combined scattering/packaging and thermal losses from phosphor downconversion. The eventual goal is to make phosphor downconversion in LEDs as efficient as linear fluorescent lighting where the total phosphor conversion efficiency, including scattering losses, is ~90%. In comparison to Task B1.3 in the 2010 MYPP for solid-state lighting, this program is designed to target correlated improvements in high temperature quantum yield and average conversion efficiency. In addition, one of the key phosphors used in this program also meets the requirements for the red spectral full width at half maximum (FWHM) thereby enabling a combination of high color rendering and lumen equivalent.

2. Progress-to-Date:

Task 2 – *Create optical and thermal model for phosphor downconversion*

Within any optical model for phosphor downconversion, two key parameters that must determined for our powder phosphors are the phosphor absorption (α) and scattering (S) coefficients. These coefficients are not readily measured from typical phosphor measurements since typical phosphor plaque measurements convolute absorption and scattering. Also, many of our phosphor samples cannot be grown as single crystals, so it is not possible to directly measure absorption coefficients. In order to experimentally determine these parameters, we have developed measurement protocols where we incorporate our phosphors within silicone films and then measure the optical properties of the films. Using a combination of in-line transmission, total transmission, and total reflectance with the inverse adding-doubling method[2], we are able to back out S and α of our phosphor particles as well as the *g*, the expectation value for the cosine of the scattering angle. In principle, S could be calculated from Mie theory for spherical particles with the phosphor particle size distribution, but our experiments have shown that these calculations tend to grossly underestimate S for blue (where our phosphor strongly absorb) and red light (where there is minimal absorption). After consultation with people familiar with these problems both within GE and at Optical Research Associates (who make the LightTools optical modeling software), one critical aspect is that typical Mie calculations are for spherical particles and our phosphors have complex polyhedral shapes with edges and facets. This affects both the

[2] http://omlc.ogi.edu/calc/iad_calc.html

phosphor scattering coefficient and the *g* value that defines the angular distribution for powder scattering.

Using this procedure, we have then measured silicone tapes that are filled with various phosphor compositions that have different activator concentrations and phosphor particle size distributions. Our measured values for α are linearly proportional to the activator concentration, are consistent with single crystal absorption measurements (when available), and do not change for different particle sizes (Table 2). All of these results are as expected. The largest change when modifying phosphor particle size is in the scattering coefficient (Table 2). We have also found that the Kubelka-Munk re-emission factor, $(1-R_\infty)^2/(2R_\infty)$, from plaque absorption can be used to scale S/α once there is a direct measurement for $S/\alpha/g$. The last point is the most critical point when running screening experiments since it is straightforward to measure R_∞ while the silicone tape measurements take additional time and effort. In addition, we have also made silicone tape measurements for phosphor blends and have found that the absorption and scattering coefficients directly scale to the specific phosphor volume fraction in the blend, again as expected.

Table 2. Relationship between phosphor particle size with scattering and absorption properties

Sample PSD	A(467)	K-M re-emission	S (mm^{-1})	α (cm^{-1})	g
2.1/10.4/22.3	0.49	0.24	10.47	91	0.915
3.9/16.0/33.7	0.54	0.31	8.18	94	0.915
7.0/24.9/49.5	0.62	0.52	5.41	94	0.923

Since we have established methods to analyze the absorption and scattering properties of our phosphors when incorporated into silicones, we use this information to understand some of the parameters that control phosphor powder scattering. The relative amount of forward scattering can be described using *g*, the expectation value for the cosine of the scattering angle. At large particle sizes, *g* should generally be independent of particle size since the particle will be much greater than the wavelength of light. We therefore wanted to determine the general region for when *g* becomes constant. The estimates reported here for phosphor particle size versus g used Mie calculations for spherical particles and assumed no phosphor absorption. Mie calculations for spherical particles have potential errors for quantitative analysis since our phosphors are non-spherical, so we only use them as a guideline for phosphor synthesis and processing. Essentially, the Mie estimates give a lower specification limit on the particle diameter of ~7 μm where there is a significant reduction in g (consequently leading to stronger backscattering). Also, for particle sizes <10 μm, the scattering cross-sections becomes significantly larger than large particle size limit of double the geometric cross-sectional area. This information is an initial input into our phosphor synthesis procedures (See Task 3).

In order to understand the effects of phosphor scattering on the performance of remote phosphor LED light engines, we have used a simple optical model that uses experimental/calculated values for the absorption and transmission of the various components in a remote phosphor package (i.e. phosphor layer, LED chips, printed circuit board, etc.) With these values, it is straightforward to generate a consistent solution by solving a system of equations for the light fluxes that are reflected and transmitted by a given layer (Figure 2). The

values for S, A, *g*, and thickness for a given phosphor layer are the input for either an adding-doubling (A-D) model or a discrete ordinate (DO) model that gives the transmission and reflectance of the phosphor layer.

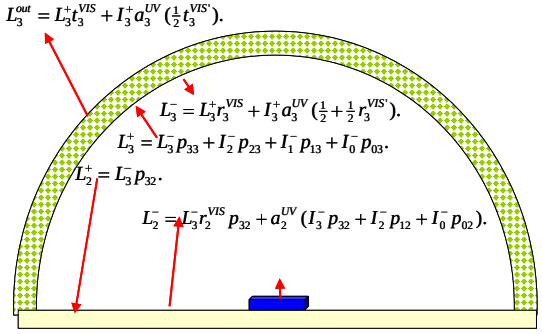

Figure 2. Schematic of remote phosphor package model

This allows us to address the effects of specific phosphor modifications on the estimated package efficiency as discussed below.

The other aspect that we have initially addressed within the modeling aspects in this program is to understand thermal quenching within LED phosphors and its relationship to activator concentration. For many LED phosphor compositions[3], there can be significantly stronger thermal quenching at high activator concentrations (Figure 3). This points to a trade-off between scattering and thermal losses since phosphor absorptions can be enhanced at high activator concentrations. In our initial studies, we have focused on the behavior $(Sr,Ca)_3(Al,Si)O_4(F,O):Ce^{3+}$ (termed SASOF)[1] and Ce^{3+}-doped garnet phosphors at high temperature and higher Ce^{3+} concentrations. In both of these phosphors, we have observed that there are minority Ce^{3+} centers whose absorption and emission bands are at lower energy and have stronger thermal quenching versus typical Ce^{3+} centers in these materials. Consequently, enhanced energy migration and transfer to these centers at high Ce^{3+} concentrations reduces efficiencies at room and elevated temperatures. Based upon the crystal chemistry in these phosphors, we have assigned these minority Ce^{3+} centers to Ce^{3+}-Ce^{3+} nearest neighbor pairs. Taking this mechanism into account[4], we are then able to estimate the onset of concentration quenching (Table 3) and the relative phosphor efficiency versus temperature. Since the probability of energy migration and the concentration of Ce^{3+}-Ce^{3+} nearest neighbor pairs both increase at higher Ce^{3+} concentrations, this points to an intrinsic limitation at high activator concentrations. For these materials, the only path to improve high temperature performance at high Ce^{3+} concentrations would be to have synthesis methods that minimize Ce^{3+} clustering effects. Consequently, our main focus going forward will be towards modify particle size distributions instead of compositions in both the SASOF and Ce^{3+}-doped garnets.

[3] Bachmann, V.; Ronda, C.; Meijerink, A. *Chem. Mater.* **2009**, *21*, 2077.
[4] Burshtein, A.I. *Sov. Phys. Usp.*, **1984**, *27*, 590.

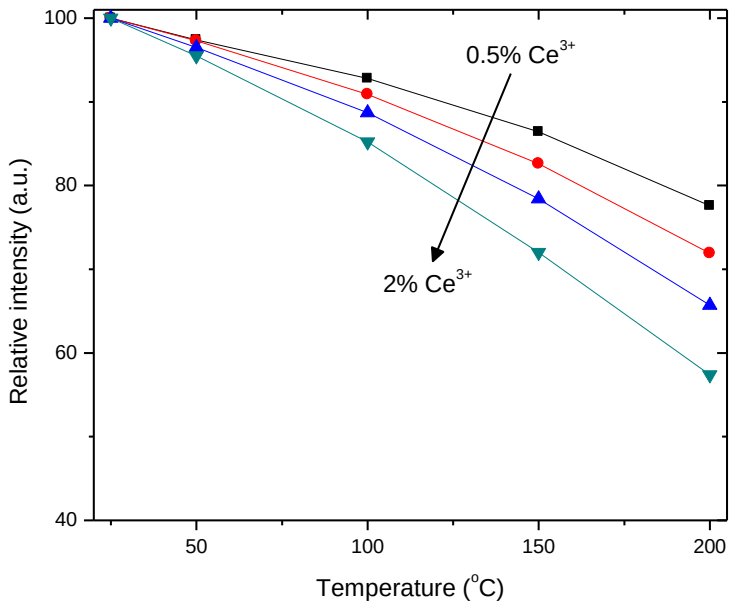

Figure 3. Thermal quenching versus Ce^{3+} concentration in SASOF

Table 3. Calculated quantum efficiency when accounting for energy migration and trapping by low efficiency Ce^{3+} pairs in SASOF.

concentration	Pair level	IH(x)	Static	Hopping	QE(static*hopping)
0.10%	1.33E-06	2.12E-05	1.00E+00	1.59E+03	**100%**
0.25%	8.32E-06	1.33E-04	1.00E+00	2.48E+04	**100%**
0.50%	3.32E-05	5.30E-04	9.99E-01	1.98E+05	**99%**
0.75%	7.47E-05	1.19E-03	9.98E-01	6.67E+05	**97%**
1.00%	1.33E-04	2.11E-03	9.96E-01	1.58E+06	**92%**
1.25%	2.07E-04	3.30E-03	9.94E-01	3.08E+06	**86%**
1.50%	2.98E-04	4.74E-03	9.92E-01	5.32E+06	**79%**
1.75%	4.05E-04	6.45E-03	9.89E-01	8.44E+06	**70%**
2.00%	5.28E-04	8.41E-03	9.85E-01	1.26E+07	**61%**
2.25%	6.67E-04	1.06E-02	9.81E-01	1.79E+07	**52%**
2.50%	8.23E-04	1.31E-02	9.77E-01	2.45E+07	**44%**

In regard to thermal models for LED systems, we initially refrained from extensive thermal modeling due to the variety of potential designs and applications. Instead, we wanted to focus upon the development of methods to measure temperatures within phosphor parts in order to give experimental values of phosphor temperatures. For these measurements, we use the properties of the red-line emitting phosphor $K_2SiF_6:Mn^{4+}$ (PFS) as an internal thermometer for our phosphor parts. Alternatively, one can use spectral characteristics to measure PFS temperatures in LED systems. One possible method again utilizes vibronic coupling to the $^2E \rightarrow {}^4A_2$ transition. This coupling leads to long-wavelength and short-wavelength emission lines that are symmetric around a zero-phonon-line (ZPL) at ~620 nm (Figure 4a). These long-wavelength and short-wavelength components are termed Stokes and anti-Stokes components and have a temperature dependence based upon the phonon occupation number for a given frequency. This temperature dependence leads to higher intensities for shorter-wavelength emission lines at high temperatures (Figure 4a), and in single-phosphor measurements, we can use these changes as an internal thermometer. However, in phosphor blends, the Mn^{4+} line emission of PFS is superimposed upon the broad luminescence bands from the other phosphors within the blend. Consequently, any analysis of the relative Stokes and anti-Stokes components

would have to involve appropriate subtraction of this broadband luminescence. Since emission bands for most phosphors broaden and lose intensity at higher temperatures, there will be an inevitable convolution with the changes in the other phosphors in the blend. In addition, this subtraction process would have to be redone for different phosphor components and blends. However, apart from changes in the ratio of Stokes and anti-Stokes emission, there is a redshift in the emission wavelength at higher temperatures (Figure 4b). The redshift (in both energy and wavelength units), Δ(PFS), versus temperature (T) for the main vibronic emission line in PFS is fitted very well to a simple linear function (Figure 4c):

$$\Delta\ PFS\ = -0.1153 + 0.00495T \qquad [2]$$

This linear fit of the redshift to temperature can be qualitatively understood using the McCumber-Sturge analysis[5] for the position of the zero-phonon line versus temperature:

$$\Delta E = \alpha_n\ T\ \ T_D\ ^4 \int_0^{T_D/T} \frac{x^3}{e^x - 1}\ dx \qquad [3]$$

where α_n is an electron-phonon coupling constant and T_D is an effective Debye temperature. The McCumber-Sturge formula was initially derived for the zero-phonon (R-line) in $Al_2O_3:Cr^{3+}$ and has also applied for other d^3 ions[6], such as V^{2+}. Therefore, it should be applicable to the zero-phonon line in PFS, but the weak intensity for the zero-phonon line in PFS (Figure 4b) requires that we analyze the peak shift versus temperature in the main vibronic transition at ~631 nm. Strictly, the McCumber-Sturge formula does not apply to vibronically assisted transitions since there are additional anharmonic effects[6], but it serves as a guideline towards the relationship of peak position versus temperature, especially at high temperatures. Using an analytical solution to Equation 2, the peak shift is essentially linear (R^2>0.99) when $T>0.7T_D$ with a slope that approaches the high temperature limit of $\alpha_n/3T_D$, so a linear relationship for PFS peak position versus temperature is reasonable. Practically, it is straightforward to implement the relative PFS peak position as a thermometer within LED packages and/or systems since the sharp-line emission of PFS can be resolved over the broadband background emission of Ce^{3+} and/or Eu^{2+} phosphors (Figure 1). We will use these relationships further in the discussion for Task 4, when we assess phosphor temperatures in remote phosphor LED systems. In addition, similar measurements have been made for all Mn^{4+}-based line emitters and are important when assessing any convolutions between phosphor temperature and incident blue flux for PFS reliability.

[5] D.E. McCumber and M.D. Sturge, J. Appl. Phys. **34**, 1682 (1963).
[6] G.F. Imbusch, W.M. Yen, A.L. Schawlow, D.E. McCumber, and M.D. Sturge, Phys. Rev., **133**, A1029 (1964).

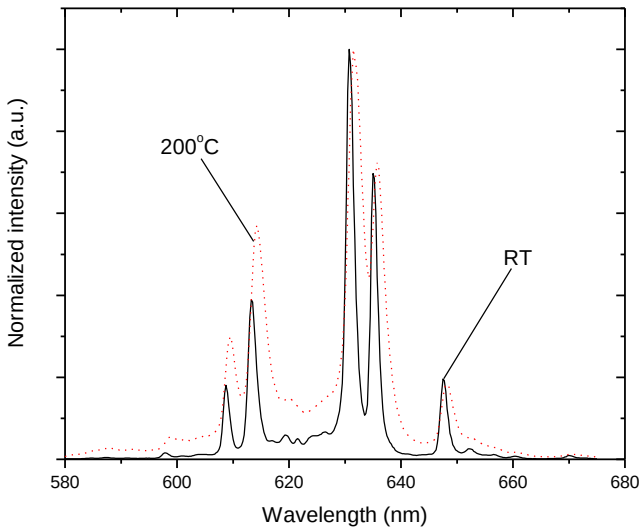
Normalized intensity (a.u.)
200°C
RT
580
600
620
640
660
680
Wavelength (nm)

(a)

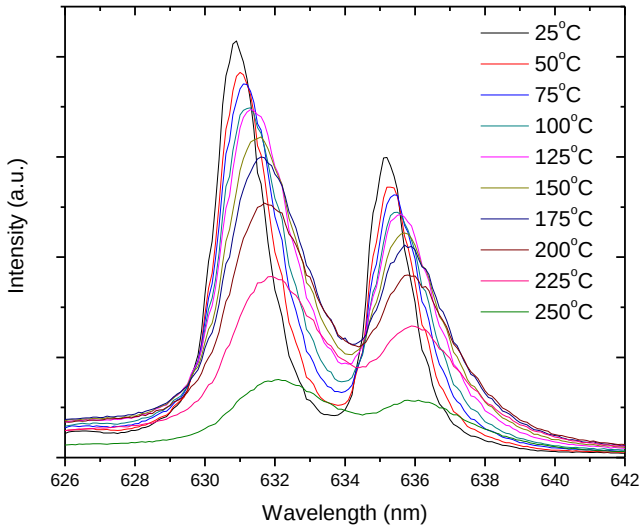
Intensity (a.u.)
25°C
50°C
75°C
100°C
125°C
150°C
175°C
200°C
225°C
250°C
626
628
630
632
634
636
638
640
642
Wavelength (nm)

(b)

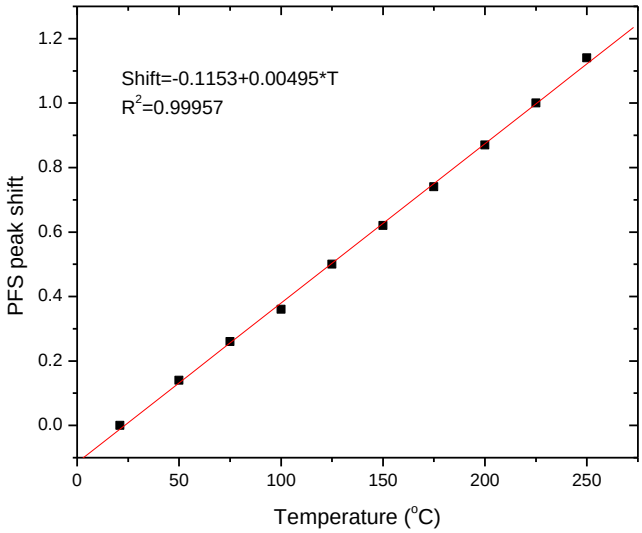

(c)

Figure 4. PFS properties versus temperature: (a) Emission spectrum versus temperature (λ_{ex}=450 nm); (b) High resolution emission spectrum (λ_{ex}=450 nm); and (c) Position of main PFS peak versus temperature with linear regression fit.

Task 3 – *Development of optimized phosphor compositions and synthesis*

Development and optimization of green phosphor compositions

As detailed above, for our SASOF and other Ce^{3+}-activated phosphors, we believe that there are thermal limitations to increasing the absorption/scattering (α/S) ratio by simply increasing activator concentrations. Consequently, we decided to modify the scattering properties of our phosphors through improved synthesis/processing of these materials. This was first done through an elutriation process where fine phosphor particles are separated through differences in their mass and/or density. This successfully removes a large fraction of the finer particles (d_{50} for fine particles is ~3-5 μm, depending upon the specific sample). Both our particle size measurements (Table 4) and SEM micrographs (Figure 5) of these samples indicate that small particles are removed by elutriation. It is important to note that while only <20% of the total mass is removed by the elutriation process, the scattering coefficient is 40% larger for the non-elutriated sample while the absorption coefficient remains constant within the errors of the measurement (Table 4). Accounting for this change in phosphor scattering can lead to potential improvements of 5-10% in package efficiency for 80-90% reflectivities throughout the entire package. This gain will always be much larger when there are larger absorption losses within the LED package (Figure 6). In the next section, we also demonstrate some of the improvements in LED packages after elutriation. Given these results from the elutriation process, we have adopted this elutriation process for all phosphors that will be tested in LED lamps and light engines.

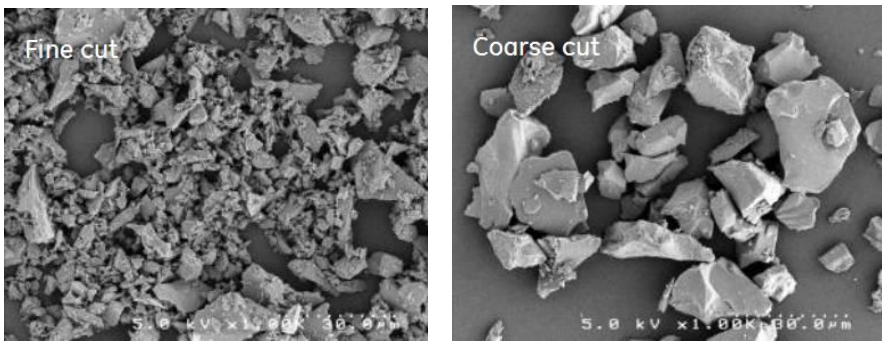

Figure 5. SEM micrographs of fine cut particles removed by elutriation process and coarse cut particles that remain from a SASOF (0.75% Ce^{3+}) phosphor.

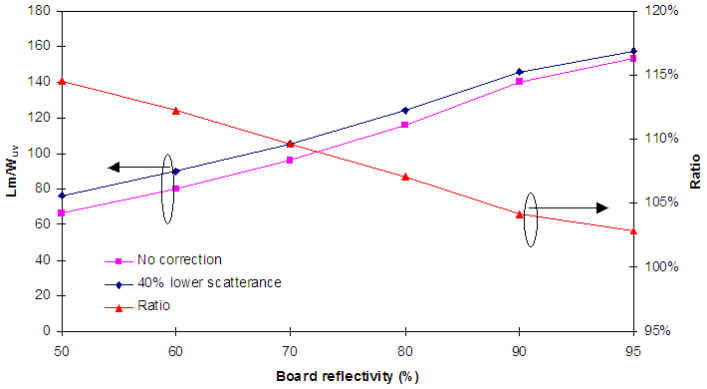

Figure 6. Potential gains versus LED circuit board reflectivity for a typical phosphor and one with a 40% reduction in the scattering coefficient.

Table 4. Properties for elutriated SASOF (0.75% Ce^{3+}) phosphor. The S values represent the scattering coefficient from a ~0.41 mm thick tape containing 0.5 g SASOF/10 g silicone.

Phosphor	**$d_{10}/d_{50}/d_{90}$ (µm)**	**S (mm^{-1}) @467 nm**	**A (cm^{-1}) @ 467 nm**	***g* @ 467 nm**
Initial	3.6/13.4/25.2	7.48	125	0.908
Elutriated	6.6/15.6/28.1	5.61	135	0.912

Within the synthesis of our blue-green garnet phosphor (termed CaSiG), we have been evaluating synthesis parameters in order to improve phosphor quantum efficiency as well as reduce the presence of scattering phases within these materials. This has included the screening of a variety of chloride and fluoride fluxes as well as varying the nominal stoichiometry of the phosphor. Our work with fluxes has not yielded any significant improvements in either phosphor quantum efficiency or plaque absorption. We believe that this possibly indicates that one limiting factor in the phosphor efficiency/absorption/scattering is the presence of secondary phases within this material. Within the synthesis of the CaSiG garnet phosphor, we investigated the effect of non-stoichiometric compositions on the phosphor quantum efficiency and absorption. We have generally found that non-stoichiometric compositions lead to higher

absorption values for these phosphors. X-ray diffraction analysis of these non-stoichiometric phosphors do not show any changes in the garnet lattice parameter, so we believe that the primary changes are in second phase concentration and Ce^{3+} segregation within these second phases. We have also found that the high temperature quenching of non-stoichiometric CaSiG compositions is slightly higher (2-3% at 150°C) than that for stoichiometric compositions. While this difference is at the limits of our instrument capability, slightly higher thermal quenching in garnet phosphors is one potential indication of a higher Ce^{3+} content[7].

Apart from direct synthesis methods, we also developed methods to remove fine particles, typically defined as those less than 5 μm in diameter, from our phosphor samples. This work has involved decanting methods that are considerably simpler in comparison to our elutriation procedures. While the methods are considerably simpler, the essential results are the same in that we measure significant improvements in the phosphor plaque efficiency and plaque absorption (Table 5). When testing these phosphors in our light engine test-bed, we observe that the fraction with larger particles have a significantly higher quantum efficiency versus the fraction with fine particles (Table 5). Since the fraction of finer particles makes up only 10-20% of the total phosphor mass, the overall improvement in the phosphor efficiency in light engine is ~3-4%. Using these methods, we have measured phosphor quantum efficiencies that are greater than 85% for the phosphors that we have optimized in this program (Table 6). These quantum efficiencies are within ~2% of the YAG:Ce industry standard phosphor. These samples have been shipped to GELS for lamp and reliability testing.

Table 5. Comparison of SASOF phosphor fractions after decanting

Phosphor	Relative QE	Absorption	Particle size (μm)
As milled	100	73	5.4/17.8/34.2
Coarse fraction	106	74	6.8/18.5/33.8
Fines	78	59	1.6/4.6/10.8

Table 6. Comparison of phosphor quantum efficiencies measured in light engines

Phosphor	Quantum efficiency (%)
YAG	89
SASOF	88
CaSiG	87-90

Apart from just efficacy concerns, we addressed additional issues within our green phosphors concerning reliability. In our SASOF phosphor, some compositions can degrade in the Vio™ prototypes under high temperature, high humidity (HTHH) conditions. Therefore, in order to address this potential issue, we have developed coating technologies to hermetically protect these phosphors from HTHH degradation (Figure 7). At this point, we have successfully screened coatings based upon a variety of inorganic oxide chemistries that significantly reduce the HTHH degradation of SASOF. When testing the optical properties of the coated SASOF phosphors, we

[7] V. Bachmann, C. Ronda, A. Meijerink, Chem. Mater. **21**, 2077 (2009).

have observed no significant changes in the phosphor quantum efficiency or in the S/α/g for coated and uncoated phosphors.

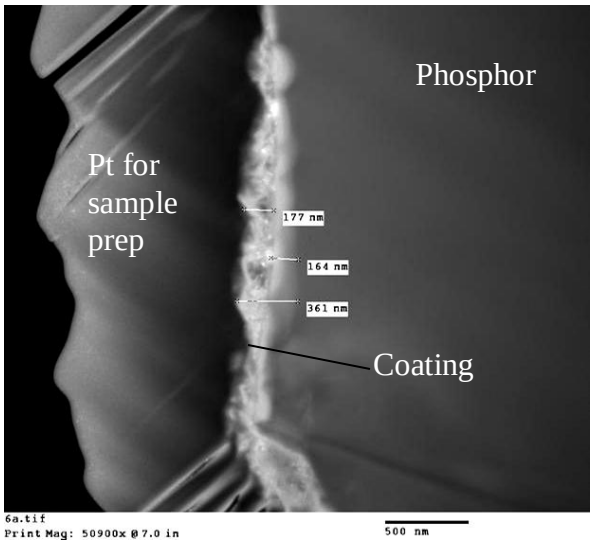

Figure 7. TEM micrograph of oxide coating on SASOF phosphor for moisture protection

We synthesized larger batches for coating the $(Sr,Ca)_3(Al,Si)O_{4+x}F_{1-x}:Ce^{3+}$ (SASOF) blue-green phosphor for moisture protection. In the coating synthesis process, we observed that a small portion of the phosphor remained at the bottom of the beaker and was likely not stirred. This part was separated from the rest of the sample and also tested for HTHH stability. We observed that this part of the "coated" SASOF that remained on the bottom of the beaker had significantly worse HTHH stability versus sample that was stirred and reacted throughout the beaker (Table 7). These results point to stirring/agitation guidelines for the coating of larger scale batches to prevent particle settling.

Table 7. Degradation of coated SASOF under HTHH conditions (~100 hrs)

sample ID	Abs.	QE	Abs.*QE	HTHH%	Abs*QE*HTHH	Comments
gc0217A1	82.9%	109.7%	124%	93	120%	50 g batch
gc0217a2	80.6%	109.8%	121%			
gc0217b1	83.2%	107.9%	122%	93	119%	50 g batch
gc0217b2	82.3%	105.3%	118%			
gc1108d1	79.0%	105.1%	113%	88	104%	6 g batch
gc1108d2	79.2%	102.9%	111%			
gc0107u1	83.6%	110.4%	126%	8	10%	Uncoated sample
gc0107u2	81.4%	108.9%	121%			
gc0217Abot2	85.0%	111.4%	129%	16	22%	Beaker bottom
Philips SAE	73.4%	100.0%	100%	96	100%	reference

In addition, from our initial synthesis of coated SASOF phosphors, we tested to see if the coating chemistry developed for one SASOF composition was applicable to alternate SASOF compositions that would be useful to optimize CRI and/or matching to LED wavelengths. In our initial tests, it appears that a protective coating is formed on the SASOF surface with minimal changes to the coating morphology, and this coating again protects against HTHH degradation (Table 8).

Table 8. Results of HTHH degradation for different SASOF phosphors before and after coating

sample ID	%HTHH	Comments
GC217A1	94	Coated batch of 2nd SASOF
GC0322	97	Coated batch of typical SASOF
GC0302	64	Uncoated typical SASOF
SAE	98	control

We also started to evaluate some aspects of the reliability of this garnet phosphor as well. Initially, given the reliability of typical garnet phosphors and the hydrolytic stability of this material, we had little concern about the phosphor reliability. However, during spectroscopic measurements of low Ce^{3+} concentration samples, we observed some phosphor discoloration upon excitation at ~350 nm (Figure 8). This degradation at 350 nm was reduced for higher Ce^{3+} concentration samples (Figure 8), and did not occur at blue wavelengths which would be relevant to this program. We have not observed any degradation in our plaque testing apparatus as well, but this serves only as a screening tool. Given the absorption bands of the garnet phosphor, we initially believe that this degradation is due to secondary phases within these materials and are not relevant at LED wavelengths (Figure 9). This is also confirmed by our typical plaque reliability tests, where we do not see any degradation in phosphor brightness after >100 hours of irradiation by 405 nm LEDs.

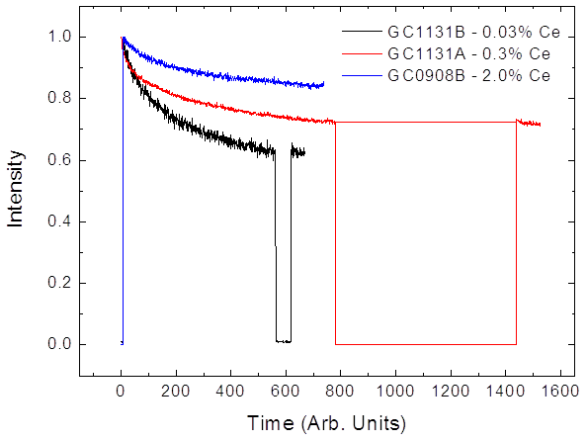

Figure 8. Degradation of blue-green phosphor with varying Ce^{3+} level under 350 nm excitation.

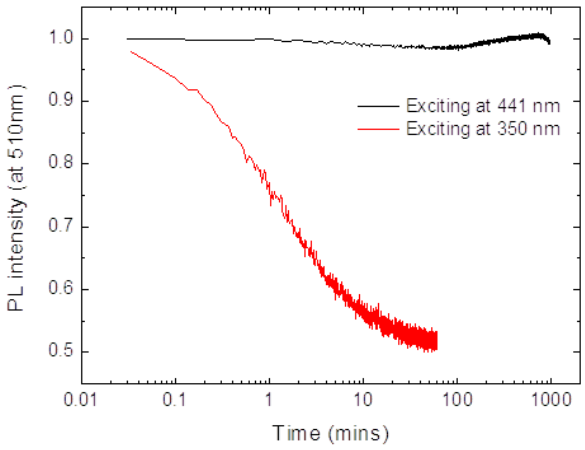

Figure 9. Comparison of degradation versus wavelength for blue-green phosphor at the lowest Ce^{3+} concentration studied.

Finally, we have also been testing alternate $SrCO_3$ and $CaCO_3$ sources for these phosphor to determine if there are any improvements and/or cost reductions for alternate sources. Currently, we are using 99.999% $SrCO_3$ and $CaCO_3$ sources from Aldrich that cost ~$4,000/kg; using these sources could make overall phosphor costs prohibitive, especially in remote phosphor applications where phosphor usage is increased. We have now tested alternate sources of $SrCO_3$ and $CaCO_3$ whose overall purity is 99.9% but are luminescent grade precursors. In these starting materials, the impurities are generally other alkaline-earth ions whose presence should not affect the quantum efficiency of the SASOF or CaSiG phosphors. In our initial experiments, we find this to be the case (Table 9). Using this information, we have begun work with toll vendors in Pennsylvania to test for larger scale-up of these phosphors. Our initial work with these toll vendors have been successful in that 100g samples whose quantum efficiency matches that of our best samples.

Table 9. Comparison of alkaline-earth carbonate sources in CaSiG synthesis

sample ID	Abs.	QE	Abs.*QE	d10/d50/d90 pre	d10/d50/d90post
Aldrich CaCO3	73.5%	91.8%	76.7%	1.8/13.7/29.3	5.8/16.1/31.9
Alfa CaCO3	75.9%	92.6%	79.9%	3.0/19.3/39.1	7.1/19.1/37.4
puratronic AA CaCO3	72.3%	89.4%	73.5%	2.6/17.9/37.5	6.7/18.4/36.7
GTP CaCO3	74.6%	93.5%	79.3%	1.9/13.9/30.7	6.4/16.6/32.0

Development and optimization of orange-red phosphors

Orange-red nitride phosphors

Apart from elutriation methods, we have also investigated synthesis methods to control particle size without milling and elutriation steps in our yellow-orange nitride phosphors. These phosphors have small particle sizes (d_{50}~4-5 μm) as well as a high index of refraction (>2.1). These phosphors also have a trade-off between activator concentration and thermal quenching, similar to SASOF and the Ce^{3+}-doped garnets, but we cannot assign a root cause for this quenching. We have measured a much higher scattering coefficient for these phosphors (as a

function of vol%) than SASOF or YAG, and there is a much lower value for *g*, the expectation value for the cosine of the scattering angle. In principle, higher firing temperatures lead to sintering and particle growth, but we have found that higher firing temperatures significantly reduce the room temperature phosphor efficiency. Therefore, we have screened flux systems that enhance diffusion and particle growth. Our fluxes are selected to have low melting/eutectic points that have components that should not incorporate into these phosphors based upon ionic size considerations. For the orange nitride phosphor, we have found one flux that can increases phosphor particle size (Figure 10) without over-sintering the phosphor cake, making it difficult to process. This fluxing process has not apparently modified the phosphor optical properties, but the larger particle size will reduce scattering coefficients. Consequently, we have the option to reducing activator concentrations and reducing the thermal quenching of this phosphor. One drawback with this fluxing technique is is that the fluxes are volatile, thereby reacting with the components in our high temperature furnaces. This limits the overall lifetime of these components. However, given the much higher performance of LED systems using our red-line emitting phosphors, we decided to stop work on these nitride phosphors.

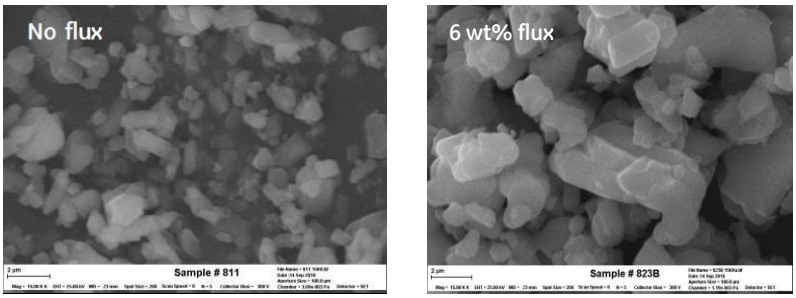

Figure 10. SEM micrographs comparing nitride phosphor samples made with & without fluxes.

Our primary goal for red phosphor was the development of synthesis processes and scale-up for the $K_2SiF_6:Mn^{4+}$ (PFS) red line-emitting phosphor. When evaluating our internal Mn^{4+}-doped complex fluorides, we observed that there was some parasitic absorption in the visible region that reduced phosphor/package efficiency and is one potential cause for reliability issues. Therefore, we have worked with a vendor to attempt to make K_2MnF_6 in a solid-state fluorination reaction that has the potential to be significantly cleaner than wet chemistry methods[8]. We have evaluated our vendor's progress in making K_2MnF_6 through fluorination routes, and they have made essentially single-phase formation of K_2MnF_6 without the presence of Mn^{3+} containing secondary phases (Figure 11). In these materials, we have now developed synthesis methods for our line-emitting fluorides using this new K_2MnF_6 precursor. Currently, we observe very little parasitic absorption in the phosphors that we make using this precursor (Figure 12), so this was thought to be a reasonable path for phosphor optimization. However, our initial decay time measurements indicate a slightly faster decay time for these materials versus some previous samples made through internal GE programs (Figure 13). This is an indication for lower phosphor quantum efficiencies, so we are investigating the potential causes for these differences. One potential cause is Mn^{4+} concentration quenching since the Mn^{4+} level in the typical crystallization method to make this phosphor[1] is not exactly known. Our estimates for the relative Mn^{4+} level in our new phosphors is roughly double that of our older phosphors

[8] P. Bukovec and R. Hoppe, J. Fluorine Chem. **23**, 579 (1987).

from plaque measurements of phosphor reflectance. Consequently, we have taken next steps are to synthesize this material with lower Mn^{4+} concentrations. We synthesized a variety of materials that varied both Mn content as well as starting precursors in order to understand the potential effects on phosphor/light engine efficiency. We have observed that nominal Mn concentrations >3.5% lead to quenching as measured by a combination of decay time, plaque quantum efficiency measurements, and light engine efficiency measurements. However, testing under high temperature, high humidity (HTHH) conditions show that these samples have comparable or better stability (Table 10) to some of the potential commercial vendors of this phosphor. In addition, the phosphor efficiency also appears to be better than that of the materials from the potential commercial vendors.

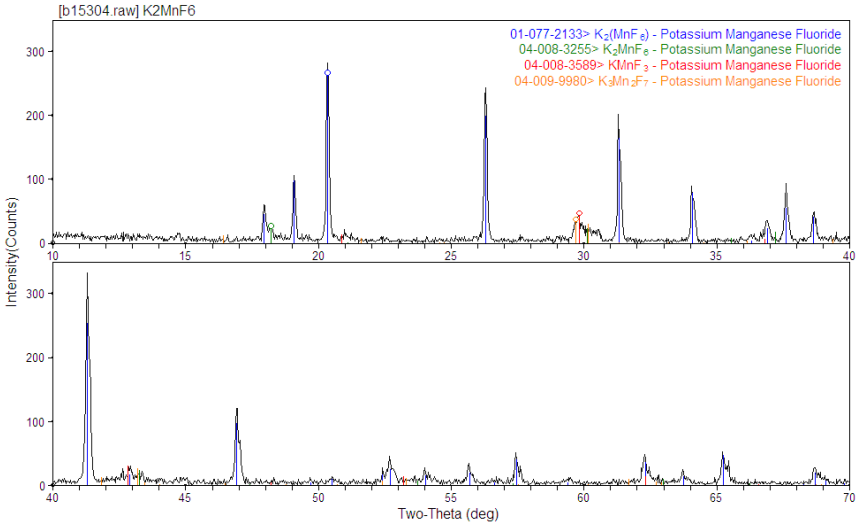

Figure 11. Powder x-ray diffraction of K_2MnF_6 made via solid-state routes.

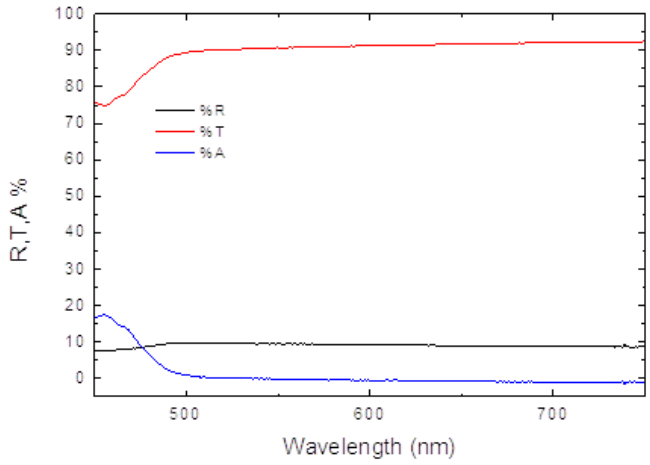

Figure 12. Reflectance (%R) and transmission (%T) and absorption (calculated as 1-%R-%T, labeled as %A) of Mn^{4+}-complex fluoride phosphor incorporated into a silicone tape.

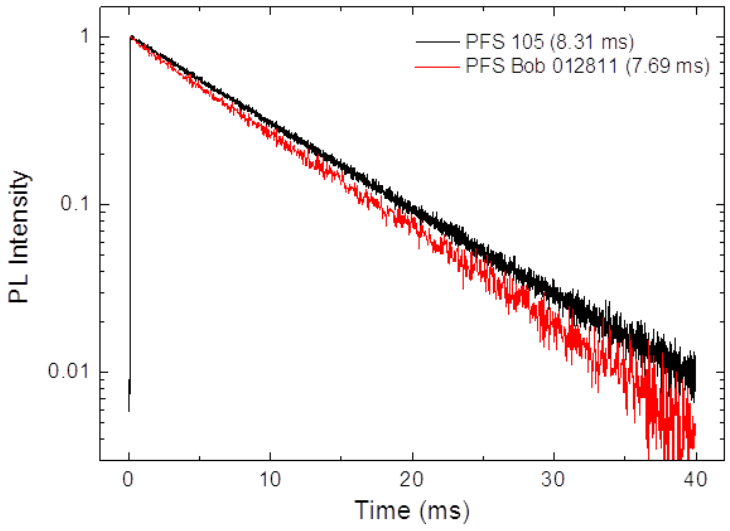

Figure 13. Decay time (λ_{ex}=454 nm) comparing K_2SiF_6:Mn phosphors made under prior GE programs (PFS 105) and those using new methods that minimize phosphor absorption in the visible (PFS Bob 012811).

Table 10. Degradation of $K_2SiF_6:Mn^{4+}$ made using a new synthesis route in comparison to previous $K_2SiF_6:Mn^{4+}$ phosphors.

Phosphor	**HTHH degradation after 48 hours**
GRC sample#1	-1%
GRC sample#2	-4%
Commercial small-scale sample	-5%

One item is that we initially observed lower efficiencies in our PFS synthesis using the K_2MnF_6 precursor made by direct fluorination. From ICP analysis of this phosphor, this synthesis process also leads to transition metal impurities due to the reactor chamber and/or mixing media. We are currently working with this vendor to reduce/eliminate these impurities. It is possible to further reduce transition metal impurities by re-crystallizing K_2MnF_6 in KHF_2/HF solutions. However, all of our PFS synthesis processes significantly removes these impurities from the final phosphor to below ICP detection limit. Consequently, we did not pursue additional modification of the K_2MnF_6 precursor in 2011.

We sent to GELS our initial samples of the PFS red phosphor made via our new process using the K_2MnF_6 precursor made by direct fluorination. While the initial lumens for this material were promising, we observed a significant change in the lamp color point and lumen loss from this material in both room temperature, operating life (RTOL) and high temperature, high humidity (HTHH) testing (Table 11). These losses/changes can be directly assigned to a loss in the red phosphor component within the blends (Figure 14). This is rather disappointing given the initial plaque tests under HTHH conditions. We therefore made initial experiments around the following factors:

- Synthesis using wet-chemistry prep for K_2MnF_6 & current co-ppt methods

- Synthesis using methods that remove ionic impurities that are come from the $(SiF_6)^{4-}$ precursor used in these experiments
- Additional washing/treatment steps to remove residual surface Mn on the phosphor particles

Table 11. Initial RTOL testing in Vio™-like prototypes using blue LED + yellow phosphor + K_2SiF_6:Mn from GRC made using a new synthesis route.

RTOL testing	Lumens	x	y	CCT
0 hrs	404.7	0.4007	0.3588	3392
285 hrs	389.8	0.3965	0.3574	3485

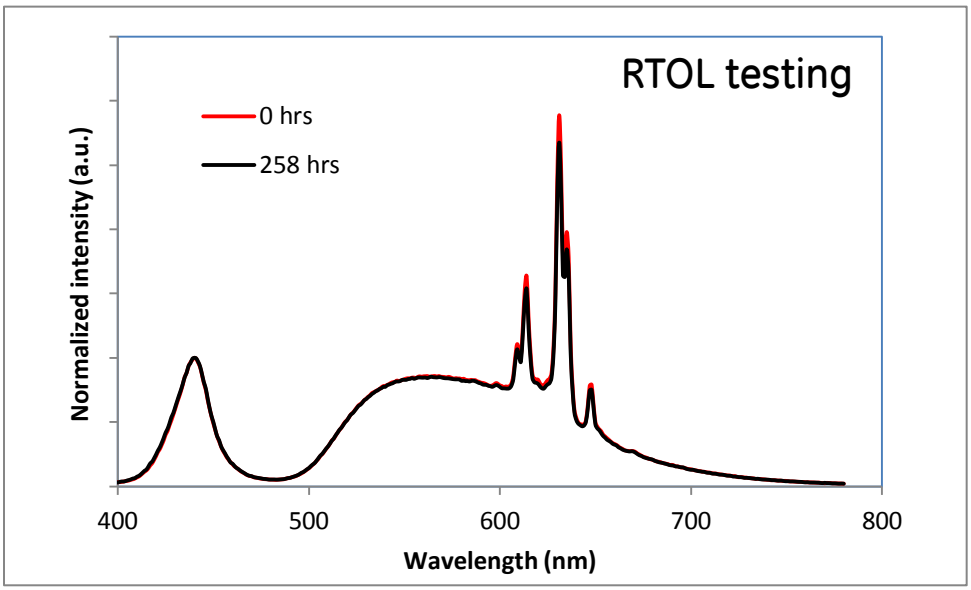

Figure 14. Spectral power distribution vs. time for lamp made at GE Lighting Solutions and tested under room temperature, operating life (RTOL) conditions.

As previously detailed, we have observed some ionic impurities that were due to our synthesis process in this material. We have also observe in thermogravimetric analysis (TGA) that these phosphors have a mass loss starting at ~120°C using a heating rate of ~5°C/min (Figure 15). Samples without these impurities do not show significant mass loss until ~600°C. In addition, mass spectrometry of the species coming off of these phosphors indicates that the mass loss is from a H_2O and OH/NH_3 species. Since all of these species could attack the PFS phosphor, this is a potential root cause for the degradation of this material. While this hypothesis is generally reasonable given the chemistry of the PFS phosphor, we must note that we have not observed similar degradation in off-line laboratory experiments to this point. The degradation of PFS remains an open issue and a concern for future experiments and testing, and we will return to this point during the discussion for Task 4.

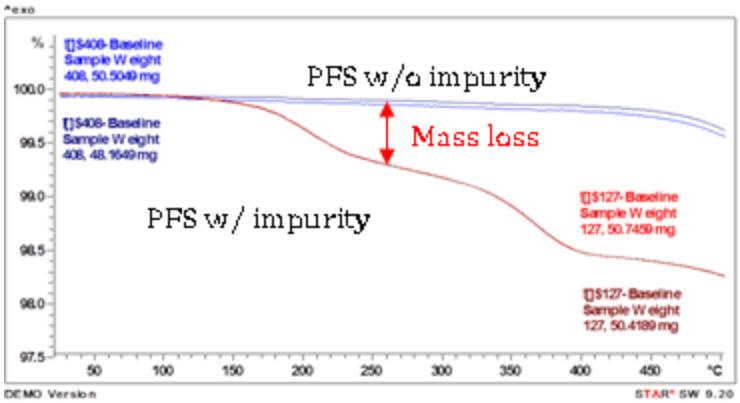

Figure 15. TGA for PFS phosphors made using two different procedures with one phosphor having an ionic impurity identified by FTIR measurements.

Taking the indication that ionic impurities play an important role in the reliability of PFS, we modified our synthesis process to remove these ionic impurities by switching our $[SiF_6]^{2-}$ source. This did not significantly change the room temperature quantum efficiency or HTHH stability of these phosphors versus our previous synthesis. Using the modified synthesis process discussed in the previous report, we have also evaluated the scale-up of this phosphor to a 75 g batch size using an external vendor in Oklahoma. The initial sample from this external vendor had a yellow-orange body color as would be expected from PFS, but there were some discolored phosphor particles within this sample (Figure 16a). Initial x-ray diffraction analysis indicated that this discoloration came from residual K_2MnF_6 that either did not dissolve in the initial precipitation solution and/or was not washed out in our treatment procedure (Figure 16b). Also, we noticed that a significant portion of these darker particles had very large sizes and could be removed by sieving. Given this assignment and observations, we then sieved the as-received phosphor and re-treated this phosphor in order to remove residual K_2MnF_6. This procedure significantly improved the phosphor efficiency and stability under high temperature, high humidity conditions (Table 12), and the properties of this phosphor made at 75 g scale generally match the properties of 12 g scale phosphors made at GE. In addition, we have communicated these findings to our toll vendor in order to improve the performance of the next large batch of PFS.

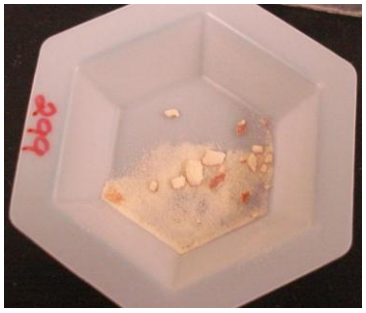

(a)

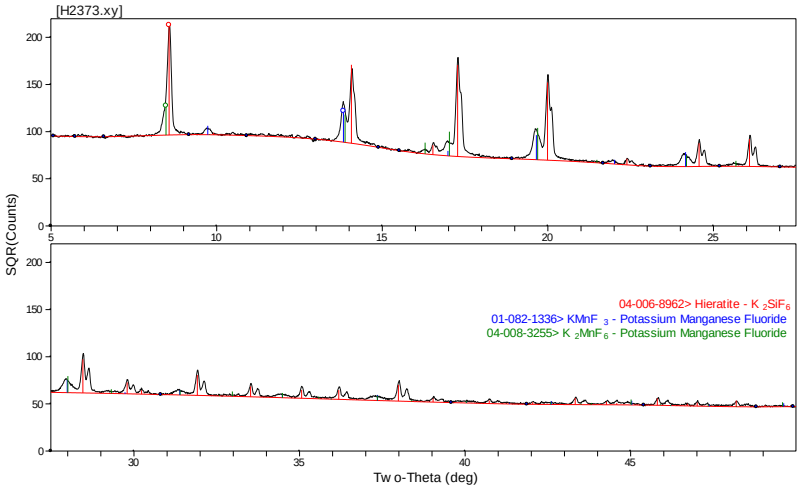

(b)

Figure 16. (a) Discolored particles from larger scale synthesis of PFS phosphors made at ARC Chemicals; (b) X-ray diffraction of powder scraped from discolored phosphor particle.

Table 12. PFS phosphor efficiency and stability versus treatment conditions from larger-scale PFS synthesis

Phosphor	**QE/Abs (450 nm)**	**HTHH stability (86 hrs)**
Untreated large batch	92/64	93%
Sieved large batch	92/64	92%
Treated & sieved large batch	102/61	109%

Apart from the synthesis of the PFS phosphor, we also studied how to potentially reduce its particle size to address future issues when processing/incorporating it into lamps. We have taken a very large particle size PFS made by another external vendor (in-kind sample provided through internal GE projects) and mechanically milled the sample either by dry or wet milling using ZrO_2 media. Our first observation is that the milling process significantly reduces the particle size much more quickly versus typical oxide and/or (oxy)nitride phosphors (Table 13), likely due to the softness of the fluoride host. In addition, there is a rapid degradation of the phosphor efficiency with milling, independent of milling environment (Table 13). The phosphor decay time does not change with milling, indicating that this loss is due to a parasitic absorption. This is supported by a measured increase in parasitic absorption at ~630 nm in diffuse reflectance measurements. Therefore, we surmise that the mechanical milling breaks up these particles such that K_2MnF_6 is now at the particle surface causing discoloration and parasitic absorptions that reduce phosphor efficiency. In order to recover this efficiency, we experimented with re-treating the milled phosphor samples in order to remove this absorption as well as varying the milling liquid for the wet milling process. However, these experiments for mechanically reducing the particle size of these materials have been unsuccessful. We first modified the milling liquid, including 40% HF and saturated solutions of K_2SiF_6/40% HF. In

these experiments, reducing the d_{50} particle size from 72 μm to 40 μm led to a reduction in the plaque quantum efficiency of >20%. Attempts to re-crystallize the particle surface by heating and cooling the milled particles in saturated solutions of K_2SiF_6/40% HF also did not improve the phosphor plaque quantum efficiency. These experiments lead us to believe that PFS particle size can be best controlled through the precipitation process and not through mechanical milling steps. Therefore, we stopped this investigation into mechanically milling PFS, and have continued our efforts towards optimizing the precipitation of these phosphors.

Table 13. PFS phosphor efficiency and particle size versus milling conditions for external sample with large particle size.

Sample	QE/Abs(450)	Decay time (ms)	d_{50} particle size (μm)
As received	100/90	8.7	73
Mortar & pestle for 3 min	64/60	8.6	23
5 minutes wet milled in acetone	67/70	8.6	22
5 minutes wet milled in ethanol	61/70	8.6	24

We first attempted to modify the pH of the precipitation solutions to determine if there are any relationships between pH and phosphor efficiency. We believe that lower pH levels will lead to decomposition of the K_2MnF_6 precursor, thereby leading to brown discoloration of these phosphors. Currently, however, we have had some degree of variability in the synthesis of these phosphors in regard to their plaque efficiency, absorption and particle size both in our small scale batches and also at our toll vendor. While the phosphor quantum efficiency can be relatively constant and consistently greater than 80%, there can be significant differences in PFS usage when blending these phosphors to make white lamps. This can potentially affect the overall system costs, especially in remote phosphor systems where phosphor usage is increased. We have traced these differences directly to different Mn levels in our phosphors (Table 14). Considering that these phosphors should have equivalent amounts of Mn, the variability suggests that there is still significant work toward optimizing phosphor synthesis.

Table 14. Elemental analysis for different PFS line emitting phosphors

	Si (wt%)	95% CI	K (wt%)	95% CI	Mn (wt%)	95% CI
Sample 1	12.8	±0.1	35.2	±0.2	0.224	±0.005
	12.7	±0.1	35.2	±0.2	0.223	±0.005
	12.8	±0.1	35.5	±0.2	0.222	±0.005
Sample 2	12.8	±0.1	35.4	±0.2	0.341	±0.005
	12.6	±0.1	35.2	±0.2	0.336	±0.005
	12.5	±0.1	35.0	±0.2	0.336	±0.005
Sample 3	12.7	±0.1	35.6	±0.2	0.419	±0.005
	12.7	±0.1	35.6	±0.2	0.418	±0.005
	12.5	±0.1	35.3	±0.2	0.408	±0.005
Large scale	**12.4**	±0.1	**34.9**	±0.2	**0.285**	±0.005

sample 1	**12.6**	±0.1	**35.3**	±0.2	**0.289**	±0.005
	12.6	±0.1	**35.2**	±0.2	**0.289**	±0.005
Large scale sample 2	**12.4**	±0.1	**35.3**	±0.2	**0.749**	±0.005
	12.3	±0.1	**35.4**	±0.2	**0.744**	±0.005
	12.4	±0.1	**35.9**	±0.2	**0.754**	±0.005

In order to address this main issue of Mn incorporation, we have modified the precipitation procedure for this material, focusing upon a controlled addition of solutions that contain K_2MnF_6, the Mn^{4+} source for this phosphor. Controlling this addition prevents hydrolysis of K_2MnF_6, which can prevent Mn^{4+} incorporation into the PFS phosphor. Given that all of these precipitation processes use HF, we have had to resort to using plastic separatory funnels to add the various solutions required to make PFS (Figure 17).

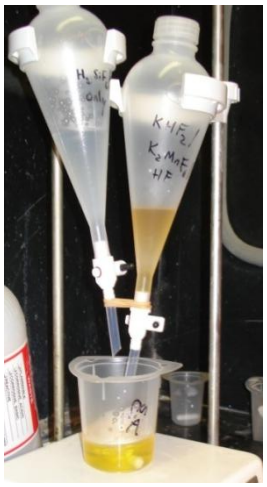

Figure 17. Picture of precipitation apparatus used for improved synthesis of PFS

Using controlled addition of solutions containing K_2MnF_6, we have also run screening experiments around solution temperatures, additions rates, and solution volumes as well. From these experiments, we have found that the major factor controlling Mn^{4+} incorporation as well as the PFS quantum efficiency is the addition rate of the solutions containing K_2MnF_6. These synthesis modifications also address the majority of the variability in our previous synthesis experiments. Consequently, we have measured absolute phosphor quantum efficiencies of ~88% for these PFS phosphors, matching or surpassing alternate commercial red phosphors (Table 15). We have taken this synthesis from 4-5 g phosphor batches to 12-15 g phosphor batches without any measurable losses in phosphor performance. In addition, we have found that post-synthesis treatment of these phosphors also leads to improved stability of the phosphor in high temperature, high humidity (HTHH) environments as described previously. All of these modifications in PFS phosphor synthesis were then given to our larger-scale toll vendor for a 50 g batch in order to verify the scale-up of these materials. Our toll vendor was able to reproduce the plaque performance of our phosphor, giving a red line emitting phosphor with an absolute quantum efficiency of 82-87%.

Table 15. Plaque measurements of GE PFS phosphors

sample ID	Abs.	QE	Abs.*QE
GE (8/2011)	63.4%	100.0%	100.0%
GE-1 (10/2011)	72.4%	105.6%	120.5%
GE-2 (10/2011)	73.7%	113.3%	131.7%
GE-3 (10/2011)	73.3%	105.1%	121.5%
Toll vendor	74.0%	106.0%	123.7%

In regard to the PFS phosphor, we have undertaken a much more extensive study of its reliability given its sensitivity to both environmental and blue flux degradation. This detailed discussion will be given in Task 4 since much of these considerations are intimately related to the LED package/light engine design.

Task 4 – *Build and evaluate LED light engines*

We discuss some of the baseline experiments in designing light engines and their effect on light output and efficacy. We have initially started by populating printed circuit boards (PCBs) with Cree LEDs that have a peak wavelength of ~441 nm. In order to have a warm white color temperature (2700-3000 K) and CRIs of ~85 and above, it is necessary to combine our red line emitter phosphor with the yellow-green SASOF phosphor, and either the orange phosphor (λ_{max}~610 nm) developed in the previous DOE program or a proprietary yellow phosphor (λ_{max}~590 nm) developed outside of the DOE programs. We conducted simple tests with these blends of these phosphors that were incorporated into silicones and then tape cast such that they are the downconverting layer in a remote phosphor geometry. The first test was using the as-received PCB that had exposed Au pads that can act as absorbing centers, and the second test essentially covered these pads with a 3M polymer film that has high specular reflection. From these initial tests, we wanted to compare the light output and phosphor efficiency when the specular reflector is placed within the light engine (Figure 18). While there are slight changes in the light engine color point, the major change is that the lumen output is >30% higher in the light engine with the specular reflector, without any changes in either the LEDs or the phosphor tapes used in these experiments. This is a clear path towards improving system level efficacy in remote phosphor systems, and this work will be combined with the materials development work described for Tasks 2 and 3 to meet our program deliverables.

Figure 18. Picture of six blue LED light engines before and after modification of printed circuit board surfaces.

Consequently, our two-flux package model was then modified to this cylindrical light engine that has flat phosphor downconversion layer versus the dome geometry shown in Figure 2. In addition, this light engine provides us with quick feedback towards the impact of improvements in our phosphor synthesis & processing. Using this engine, we did not initially expect to find significant differences between phosphors whose fine particles were removed via the elutriation process since the materials used in this light engine have reflectivities of ~98% (Figure 18). However, for our SASOF phosphor, we have found a 5-10% improvement in the phosphor quantum efficiency (as measured within this light engine) for the elutriated phosphor sample. We attribute this improvement to the removal of phosphor particles that are mechanically damaged through the milling process as is well-known in phosphor processing. Consequently, for our green phosphor samples, we measure a total package efficiency of 72-75% for phosphor downconversion in these light engines. Also, combining this value with the two-flux model allows us to estimate the phosphor quantum efficiency since the values for the phosphor reflectance/transmission in the visible can be directly measured. Using this methodology, we obtain quantum efficiencies of ~>87% for our green phosphors and 82-88% for our red-line emitter phosphors. Reaching these efficiencies is one of the milestones within our final Task 3 deliverable to have phosphor efficiencies that are greater than 85%.

We note that our cylindrical light engine, while showing improvements versus prior prototypes, is likely not sufficient to reach the deliverables within this program. Using our two-flux models, we believe that switching back to a dome-like geometry from this cylindrical engine will be critical to further improvements in the package (and therefore light engine) efficiency. Alternately, having the reflector walls having an angle (making a conical light engine) can also significantly improve light engine efficiency versus a cylindrical light engine. Our initial estimates with a phosphor dome with the same printed circuit board in the cylindrical light engine give an improvement in light engine efficiency of >10%. The rationale for this improvement is the strong reduction in package absorption in the dome system. Most high efficiency phosphors have very high reflectances in spectral regions outside of the phosphor excitation, making phosphor powders excellent reflectors. While replacement of 98% reflective materials with materials with 99% reflection seems miniscule, it is necessary to account for the multiple bounces that light will have in a warm white LED package where thicker phosphor coatings are needed. For example, if a light ray bounces 5 times off a surface before escaping the light engine, the difference between 98% and 99% reflectivity gives a ~5% difference in light output. However, realizing this improvement for a dome geometry critically depends upon removing all parasitic absorptions within the phosphor layer. This puts additional emphasis on the tasks to remove parasitic absorptions within our phosphors (Figure 12).

As noted from our results from our previous program, the Mn^{4+}-doped complex fluoride phosphor can enable both high CRIs and a high lumen equivalent rating (LER). This phosphor has been the basis of many of the high-efficacy blends reported both in the prior and current GE DOE phosphor programs. One potential drawback for this material is that its 1/*e* decay time is ~8 ms, making it susceptible to saturation at high LED fluxes. In order to test this out, we made LED packages that using 441 nm LEDs with an optical power of ~0.41 W at 350 mA and a phosphor/silicone cap with an inner diameter of ~2.5 mm versus ~1 cm for a typical Vio^{TM}

hemisphere (Figure 19). Within these tests, we ran two separate experiments where the LED drive current was varied and instantaneous efficacy measurements were made and pulsed measurements where the efficacy was measured as a function of duty cycle. We observed that the ratio between the blue LED bleedthough and red phosphor emission increased both at high currents and high duty cycle (Figure 20), an indication of phosphor saturation. This would indicate that the high LERs blends that are possible with red-line emitters are most effective in remote phosphor configurations where the incident flux on the phosphor is reduced. Our next steps will involve quantifying this saturation to understand the relationship between flux and phosphor efficiency to understand the packaging regimes for these red-line emitters. However, we have also made similar tests for white light blends using yellow-green phosphors in combination with the Mn^{4+}-doped complex fluoride phosphor (Figure 21). In these tests, the shift in the phosphor color point versus drive current would indicate stronger quenching from the green phosphor instead of the red phosphor. This does not follow the relationship that we expected for phosphor saturation since the 1/*e* decay time for the green phosphor is 50-70 ns or ~160,000x faster than the decay time for the red phosphor. In our experience and analysis, we would not expect any intensity saturation from our green phosphor. We also would not expect thermal effects in these experiments since the LEDs were on for <10 sec during the measurements and there was ~2 minutes in between each measurement. However, thermal effects are consistent with our observations since the Mn^{4+}-doped complex fluoride phosphor has <1% quenching up to 150^{o}C and all of our green phosphors have ~10% quenching at 150^{o}C. This is also consistent with our measurements of packages using only the green phosphor (Figure 22). We are therefore troubleshooting our experimental procedure in order to determine the root cause for the differences in these measurements.

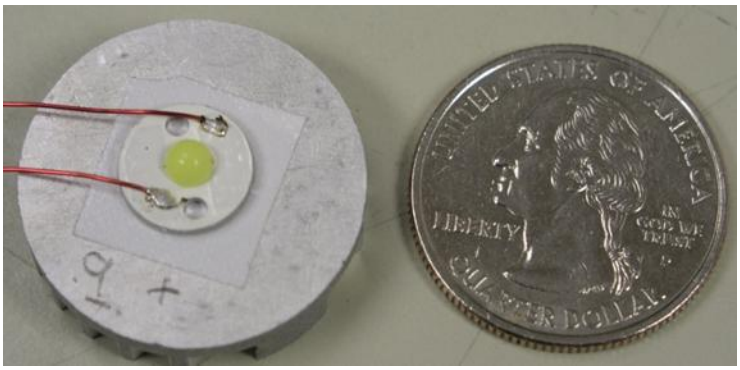

Figure 19. Photograph of package and phosphor dome for saturation tests.

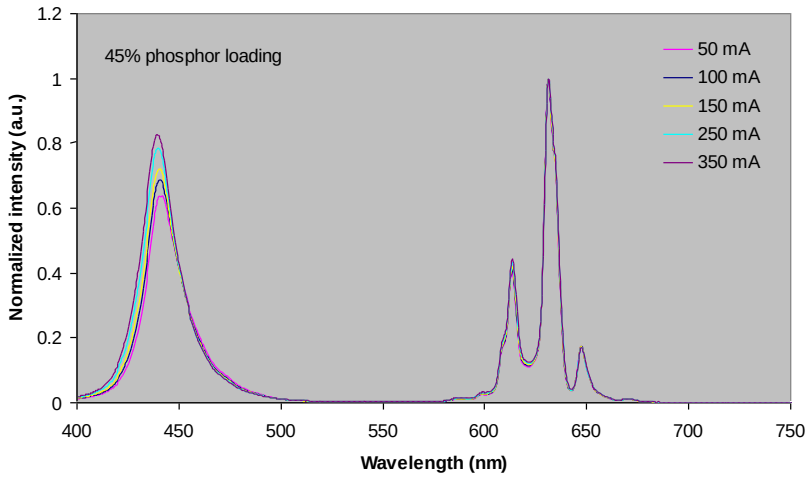

Figure 20. Emission spectra for package with red-line emitting phosphor with varying drive current.

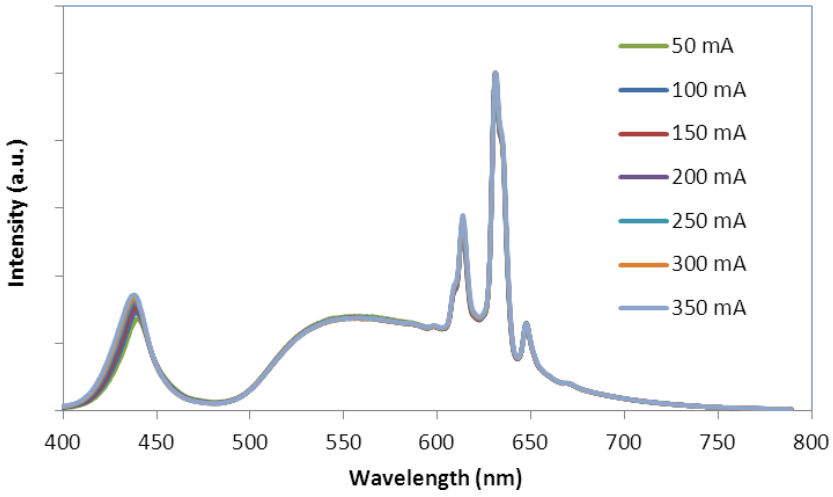

Figure 21. Normalized emission spectra for smaller package with a blend of a red and green phosphor versus drive current.

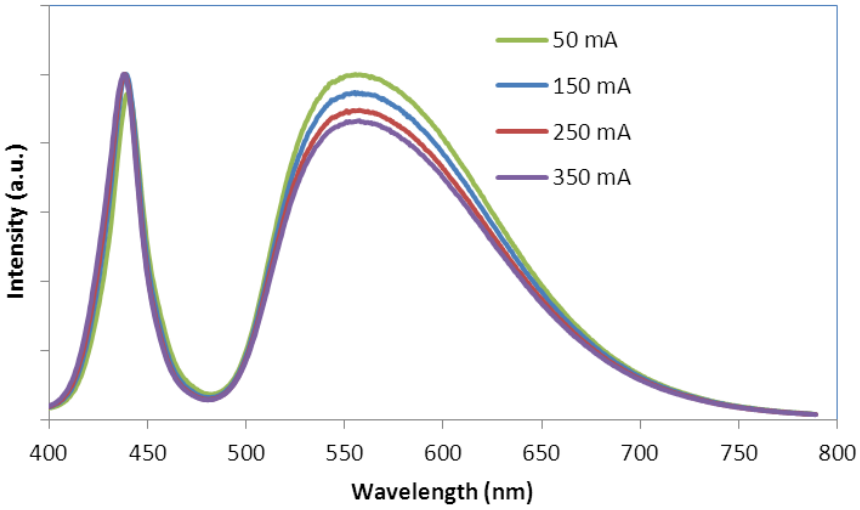

Figure 22. Emission spectra for smaller package with green phosphor versus drive current.

We continued these experiments on phosphor saturation in $K_2SiF_6:Mn^{4+}$ (PFS) line emitting phosphors by using the same 6-chip light engine previously used to evaluate board reflectivity (Figure 18). Using this 441 nm light engine, we evaluated the instantaneous phosphor efficiency versus incident optical power (Figure 23) under excitation conditions (<10 sec after turning LED power on) that minimize thermal effects. In this light engine, we observe evidence for <4% loss in phosphor efficiency at the highest fluxes measured (Figure 23). This order of magnitude is reasonable when taking into account phosphor saturation by a simple ground-state depletion mechanism [9] combined with the PFS decay time and absorption coefficient (~30 cm^{-1}). However, since PFS will be used in blends with other phosphors, the minimum flux for significant saturation losses will be higher since the incident blue LED flux will be filtered by the other phosphors in the blend.

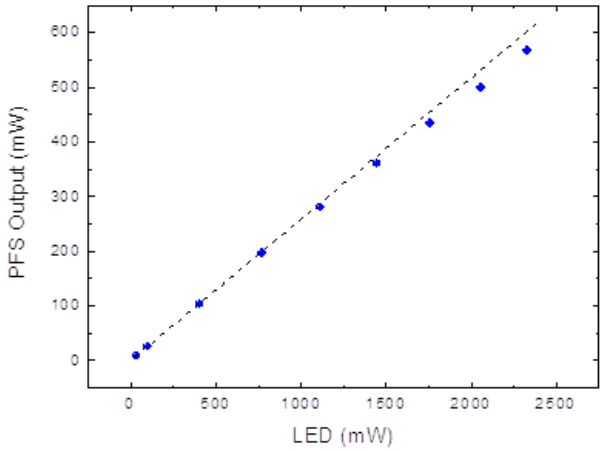

Figure 23. Optical output of PFS phosphor versus LED optical input. The dotted line signifies the linear behavior expected in the absence of saturation.

[9] S. Mikoshiba, S. Shirai, S. Shinada, and M. Fukushima, J. Appl. Phys. **50**, 1088 (1979).

In general, when PFS is used in typical remote phosphor systems, this phosphor has less than 1% loss in quantum efficiency from photosaturation. This does not address how this phosphor can be used for high CRI and LER blends. The combination of a blue-green and yellow phosphor with PFS can lead to higher CRIs and LERs even when using shorter blue wavelength LEDs that can have higher wall-plug efficiencies (WPEs) and reduced current droop[10]. Given our progress in the synthesis of the CaSiG blue-green phosphor and the K_2SiF_6 red-line emitter, we decided to start making white lamp prototypes using these materials in addition to a yellow phosphor developed under internal GE programs (termed YON). These initial prototypes used the cylindrical light engine that we have previously discussed that uses Cree EZ LEDs with a peak wavelength of ~441 nm and have a pulsed WPE of ~36% at drive currents of ~350 mA. Using this blend, we are able to reach warm-white color temperatures at extremely high color rendering (Table 16). The differences between calculated and measured blend properties are small, which also indicated that there is minimal re-absorption of phosphor luminescence by the other phosphors. While the color properties of this blend are promising, it is clear that this blend initially fell short of our program deliverable of ~200 lm/W_{blue} with the current phosphor efficiency of 145 lm/W_{blue}. However, we believed that this initial lamp made for phosphor screening purposes can be significantly improved upon in the following manner:

- Elutriation of blue-green CaSiG phosphor to remove phosphor fines that can reduce phosphor quantum efficiency and increase scattering losses. We estimate an increase in lamp performance of 3-5%.
- Use of higher quantum efficiency PFS that has reduced parasitic absorption via optimized synthesis processes. We estimate an increase in lamp performance of ~5-7%.
- Improve phosphor efficiency of YON yellow phosphor that will be done under internal GE programs. We estimate an increase in lamp performance of 3-5%.
- Switch from cylindrically shaped light engine with flat phosphor film to hemisphere phosphor dome. We estimate an increase in lamp performance of 7-10%.

Table 16. Comparison of high CRI blends using Cree EZ LEDs with 441 nm peak wavelength.

Lamp	CCT (K)	CRI	R9	LER (lm/W_{opt})	Phosphor efficiency (lm/W_{blue})
Predicted	2850	96	93	330	---
Experimental	2863	95	86	334	145

Apart from our phosphor development, it is obvious that the use of higher wall-plug efficiency (WPE) Lumileds Rebel royal blue packages would lead to significant improvement in our light-engine efficacy. We began to demonstrate this in our light engine prototypes. First, within a cylindrical light engine and a flat phosphor downconverting layer, the efficacy increases to >90 lm/W at ~2900K, 90CRI versus our prior light engines that had efficacies of ~75 lm/W. In this case, the phosphor efficiency, defined by the ratio of lumen output and incident blue LED optical powder (lm/W_{blue}), is independent of whether high WPE Lumileds packages or Cree LEDs are used in this light engine configuration. Within this system, however, there are significant losses due to the addition of the cylinder and the placement of a reflector layer on the

[10] A. David and M.J. Grundmann, Appl. Phys. Lett. **97**, 033501 (2010).

printed circuit board (PCB) (Table 17). We can expect that the placement of the reflector layer can be optimized in order to reduce this specific loss, but cylinder losses are likely to be an inevitable feature of this light engine.

Table 17. Comparison for light engine with PCB reflector and cylindrical attachment

	V_F (V)	I (mA)	Power (W)	WPE	Δ
Bare engine	8.4	350	1.68	57.1%	---
+ cylinder	8.4	350	1.53	52.0%	-9%
+ cylinder + bottom reflector	8.4	350	1.48	50.3%	-12%

The inherent losses due to a cylindrical configuration can be overcome by using a dome configuration for the phosphor downconverting part. In our simple package model, we estimated that the dome configuration would lead to a 12% improvement in efficacy due to the removal of a large amount of surface area that can absorb visible light and has no transmission. From our measurements of dome and cylindrical light engines at nominally similar color points, we observe an improvement of ~11% (Table 18), in good agreement with our package model.

Table 18. Comparison of cylindrical light engine with phosphor dome

	Cylinder with flat phosphor part	Phosphor dome
SASOF mass	150 mg	220 mg
PFS mass	279 mg	408 mg
CCT	2952 K	3009 K
dbb	0.010	0.007
CRI	91.5	91.0
Efficacy (lm/W_{blue})	185.7	198
Efficacy ($lm/W_{electrical}$)	93.4	104

The effect of the PCB reflector is reduced with the use of a dome downconverting part versus the cylindrical light engine. In these light engines, the PCB reflector improves the phosphor conversion efficiency by ~13%, while also leading to a 4-5% loss in the blue power incident on the phosphor. This leads to a total efficacy improvement of ~8%. In contrast, using a PCB

reflector in the cylindrical configuration led to efficacy improvements of ~30-40%. Through blend composition adjustment, we are able to adjust the lamp color point onto the blackbody locus. For this lamp, we are able to have efficacies >100 $lm/W_{electrical}$ (pulsed) at 2900K, 89CRI with total phosphor efficiencies of 199 lm/W_{blue}. When accounting for Stokes losses, this translates a total package efficiency of 78-80% or 10-15% higher than the package efficiency at the start of the program. In addition, given blue LED wall-plug efficiencies of ~70%, this could lead to light engine efficacies of ~140 lm/W for CCT<3000K, ~90CRI. These values are reaching the physical limits for performance given that our phosphor quantum efficiency ranges from 85-90%. At this point, our next steps were:

- Determine the trade-offs when going to 95CRI in the same package geometry.
- Assess methods to reduce the losses through the board reflector in these light engines using packaged blue LEDs while retaining high package efficiencies.
- Assess potential methods to reduce overall phosphor cost while maintaining high package efficacy. We note that this is not a direct deliverable for this program. However, any future implementation of the technologies developed in this program will have to minimize phosphor usage and costs.
- Measurements at steady-state conditions versus pulsed measurements.

After these results, we continued to test our lamp performance for high CRI, warm white light engines. Apart from the developments in this program, our internal GE programs have worked to improve phosphor QEs for yellow nitride phosphors that we use in the 95 CRI blends. These improvements have led to significant improvements in the phosphor efficiency, defined by the defined by the ratio of lumen output and incident blue LED optical powder (lm/W_{blue}). In our flash measurements using highly reflective board surfaces (Figure 24) and phosphor domes, we have phosphor efficiencies (flash) ranging from 185-210 lm/W_{blue} depending upon color temperatures for light engines near the blackbody locus with >95 CRI using seven Cree royal blue LED packages (Table 19 and Figure 25). Essentially, the improvements in our phosphors have closed the efficacy gap to between our 89-90 CRI parts that reported in August 2011 and the 95+ CRI parts that we are reporting in this report.

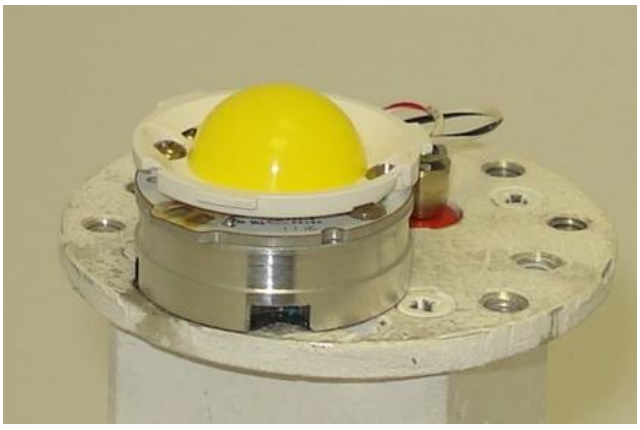

Figure 24. Picture of light engines using reflective board surfaces and a phosphor dome optic.

Table 19. Spectral characteristics for light engines with phosphor domes and specular reflecting board surfaces

CCT	CRI/R_9/dbb	Lm/W_{blue} (flash)
3750 K	95/97/0.0004	210
2850 K	96/88/-0.0008	185

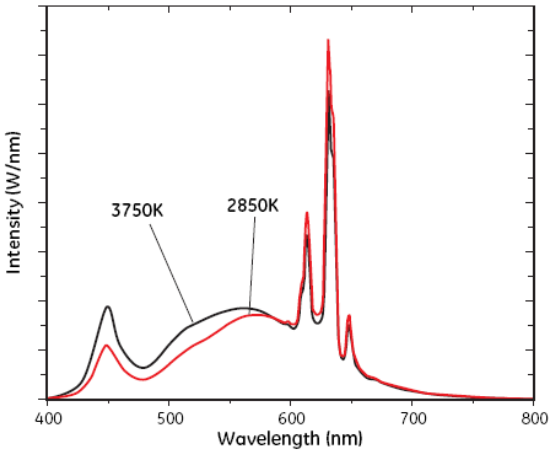

Figure 25. Spectral power distributions for 95+ CRI blends

We also made steady-state measurements to understand additional loss mechanisms due to heating of our remote phosphor parts. In order to test for an extreme case, we have made these tests at 700 mA drive currents where there is ~6 W of optical power incident on the phosphor dome. In these tests, we observe lumen losses of 15-20% from initial to steady-state measurements for the large domes (Figure 26 and 27). There are three primary loss mechanisms within these measurements:

- Reduction in LED wall-plug efficiency at steady-state (~5-8%).
- Reduction in phosphor absorption at high temperatures (~1-2%)
- Losses in phosphor QE at high temperatures (~9-12%)

The majority of these losses are in the green and yellow spectral regions (Figure 26), and accounting for the losses in phosphor QE gives an approximate phosphor temperature of ~125^{o}C for a 700 mA drive currents in these ~1" diameter phosphor domes. For smaller domes, we observe even larger losses where the phosphor temperatures are ~175^{o}C at steady-state conditions at 700 mA drive currents. Using these engines, we are also able to map out lumen losses versus light engine drive current (& therefore incident optical power) as these light engines go towards steady-state conditions (Figure 27). This information allows us to understand the different causes for thermally-induced lumen losses in our light engines. For example, we observe a correlated color shift (denoted using the y color coordinate) and lumen loss at shorter times after the light engine is turned on (Figure 28). This can be directly assigned to a loss in phosphor efficiency as the phosphor/silicone dome is heated up. At longer times, the device color stabilizes, indicating that the ratio of phosphor/blue ratio has stabilized and the phosphor dome temperature is generally constant. However, there is still additional lumen loss even with at a stable device color (Figure 28). We believe that this lumen loss could be due to additional LED losses due to higher board temperature that arise from the presence of a hot phosphor/silicone dome.

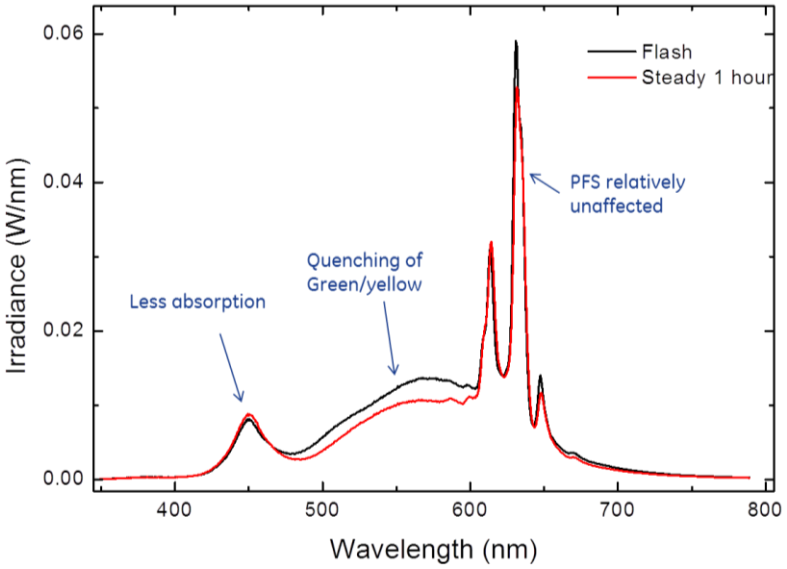

Figure 26. Spectral power distributions for high CRI blend comparing flash measurement and steady state measurements at 700 mA drive current.

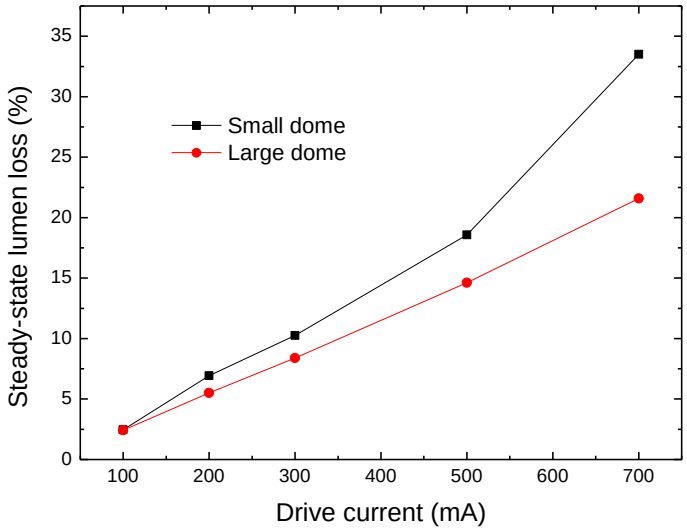

Figure 27. Steady-state lumen losses versus drive current for small (~0.78" diameter) and large (0.98" diameter) phosphor/silicone domes in a similar light engine to the one shown in Figure 24.

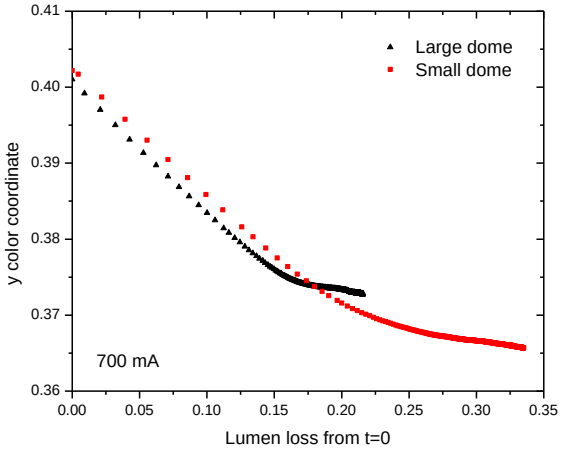

Figure 28. Plot of light engine y color coordinate versus lumen loss for phosphor/silicone domes driven at 700 mA.

We have also started modifications of the phosphor geometry to determine if there are any potential improvements in either the flash or steady-state efficacy of these light engines. Our first approach was to separate the phosphors into distinct layers, rather than a single blended phosphor layer. Since the PFS red-line emitting phosphor has less thermal quenching versus all of our other phosphors, we presumed that placing this phosphor closest to the LED could improve steady-state efficacies since this phosphor layer would experience the highest flux. Unfortunately, we did not observe any significant efficacy differences in these modifications of phosphor geometry. We note that these efficacy/phosphor efficiency values are lower than those reported above. This is because these initial experiments are for screening purposes, and we have used a sub-optimal cylindrical light engine geometry where it is significantly easier to test new concepts. Although there are no efficacy benefits, we have seen that separating the phosphors into layers can significantly reduce phosphor usage for the phosphor layer closer to the LED (Table 20). While these observations are not directly within our program scope, it will be important to reduce overall phosphor usage (and cost) in remote phosphor systems that use much more phosphor.

Table 20. Comparison of alternate phosphor geometries that separate phosphor layers using a SASOF/PFS bi-phosphor blend.

Geometry	CCT/CRI/dbb	Phosphor efficiency (lm/W_{blue})	PFS mass	SASOF mass
Typical flat disk	3040/90/0.003	152	0.223 g	0.137 g
PFS towards LEDs	3059/88/-0.003	154	0.173 g	0.115 g

Using our phosphor systems, we also have conducted baseline tests comparing our phosphors with commercially available remote phosphor systems. In these comparisons, we utilized a larger, cylindrical remote phosphor light engine with diffuse reflectors on the cylinder walls and base and replaced the commercial phosphor part with a remote phosphor part made with our optimized triphosphor blends. In these experiments, we observed that our current triphosphor blend has >10% efficacy improvements (flash and steady-state) at higher CRIs and

R_9 values (Table 21). When comparing the GE phosphor system to other commercial phosphor systems, our current efficacy at CRI>92 is generally equivalent to commercial remote phosphor systems at CRI~80-82.

Table 21. Comparison of commercial remote phosphor systems with GE phosphor systems

Phosphor disk	Lumens	CCT (K)	dbb	CRI	R_9
Commercial (flash)	905	2709	-0.003	91	73
GE (flash)	1031 (+14%)	2869	-0.003	95	93
Commercial (steady state)	879	2694	-0.004	91	72
GE (steady state)	987 (+12%)	2747	-0.006	93	89

We also have tested our phosphor systems in different light engine geometries in order to determine if there are any potential losses within different light engines. Our initial design was a 6" linear light engine that would nominally be for linear fluorescent-like fixtures and systems (Figure 29). This design is somewhat similar to the cylindrical light engine, but with sidewalls angled in order to improve light extraction. In this light engine, we have phosphor + package efficiencies of ~220 lm/W_{blue} @ 90CRI, 4000K. This roughly translates into total package efficiencies of ~85%, which will be very close to the maximum values for phosphor-based systems. These initial light engines had extremely low incident fluxes (<0.1 W/cm^2), so steady-state losses are less of an issue, and high efficacies when using high WPE LEDs (Table 22), as verified by our measurements on these light engines at GE Lighting, Nela Park. It is also possible that these light engines could also be competitive with hybrid LED systems that combine red LEDs with blue LEDs that have a yellow-green phosphor.

Figure 29. Photographs of linear light engine with >85% total efficiency.

Table 22. Efficacy versus drive current for linear light engines

Drive current	V	Lumens	Efficacy	(x,y)	CRI
150 mA	16.9 V	353 lm	**139.5 lpw**	(0.377, 0.373)	**90**
300 mA	17.7 V	677 lm	**128 lpw**	(0.376, 0.369)	**90**
450 mA	18.3 V	966 lm	**117 lpw**	(0.376, 0.365)	**90**

With the phosphors and systems developed within this program, we are close to maximum values for efficacy for CRI>90 systems. One key hurdle for the implementation of these phosphors is their reliability in LED package and systems. Among the phosphors studied in this program, we decided to focus our reliability efforts on the PFS red line-emitting phosphors since there is no substitute for this phosphor and its properties. As noted above, one key risk for PFS is its stability against hydrolysis, which is partially addressed through the optimized chemical treatment process. However, we wanted to further understand the limits of this material under ambient humidity conditions, where phosphors are more likely to operate. In short-term (~72 hour) tests, the onset for treated PFS degradation is ~100^{o}C with a lower onset for untreated PFS (Figure 30). We have extended this test further at 80^{o}C and have not seen any loss in treated PFS QE after 1000 hours of exposure. Consequently, we have more confidence in an upper-use temperature of 80^{o}C for PFS. This temperature is close to the point where most typical yellow-green phosphors begin to lose intensity, so there are multiple reasons to keep PFS-containing blends below 80^{o}C.

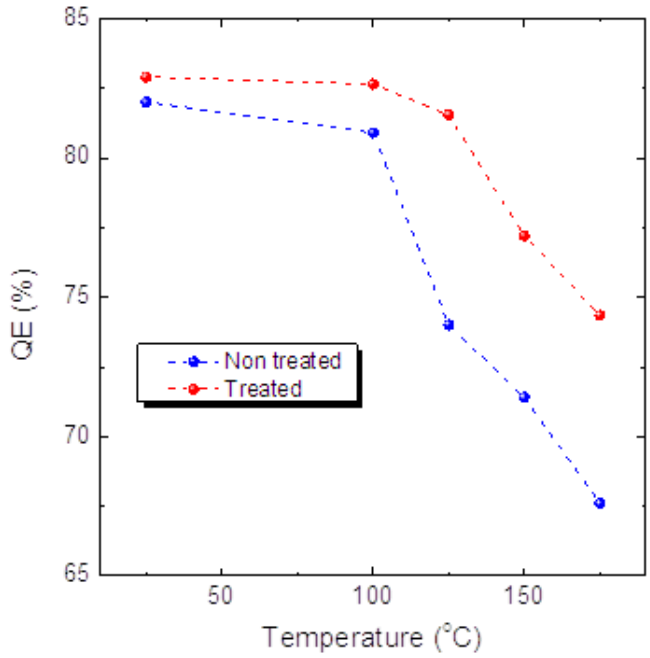

Figure 30. PFS quantum efficiency after exposure at a given temperature for ~72 hours.

Apart from hydrolysis-based degradation, we are also concerned with PFS degradation under high-intensity blue light. In order to understand these effects, we have used laser-based irradiation techniques to accelerate blue light damage of PFS (Figure 31). In these tests, we observe permanent PFS damage under blue light fluxes that are >50 W/cm^2 (Figure 32), while industry standard phosphors remain constant. In these tests, we have gone through and varied blue light fluxes and temperatures in order to initially understand the damage characteristics for PFS. We have found that the laser damage is a superlinear process that is dependent upon (flux)^N with N>1 and also has thermal activation with E_a~0.19 eV. Scaling back from >50 W/cm^2 to the <0.3 W/cm^2, T<65^{o}C values in many of our remote phosphor systems, would indicate that that PFS could be stable under these conditions, although it is difficult to extrapolate these accelerated tests out to 50,000 hours. This is supported by our tests in Vio^{TM}-like prototypes where we have demonstrated prototypes with <1 MacAdam ellipse shift and <2% lumen loss after 4000 hours of testing (Figure 33). In order to further check this, we have also placed three linear light engines based upon the design in Figure 29 for longer-term reliability testing.

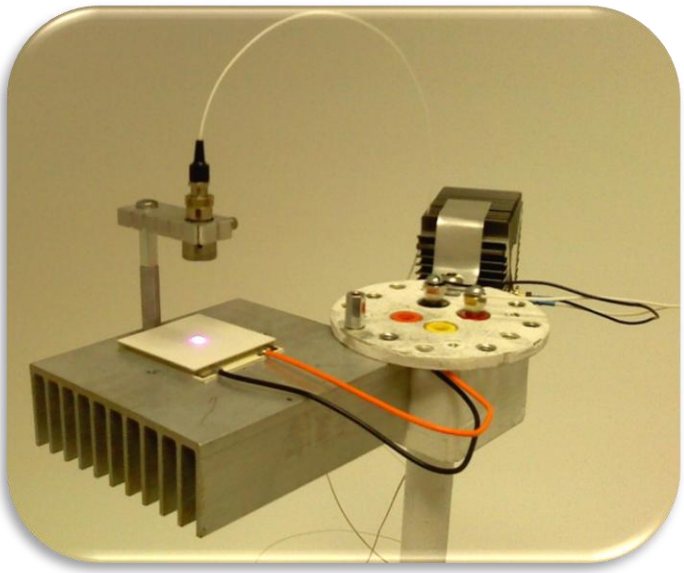

Figure 31. Experimental setup for laser irradiation of phosphor samples

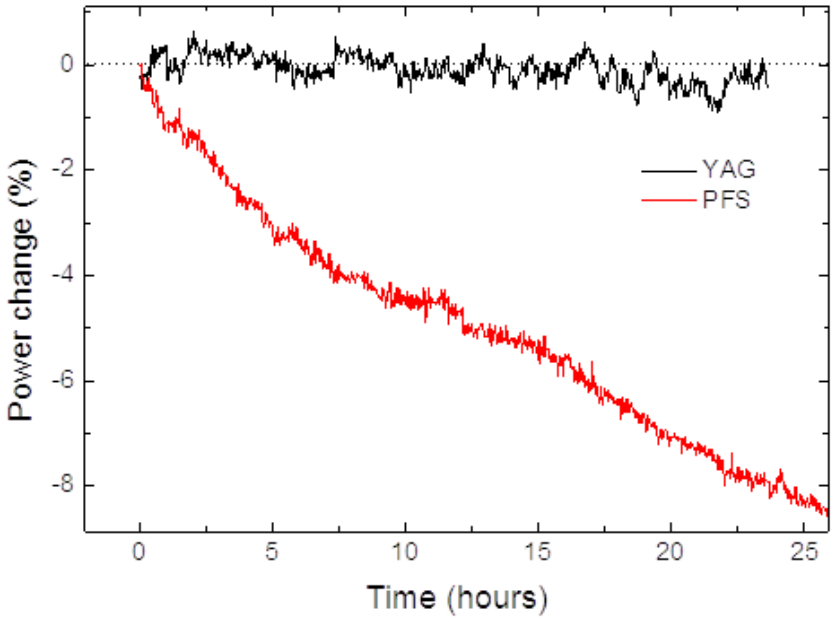

Figure 32. Comparison of PFS under laser irradiation versus YAG:Ce

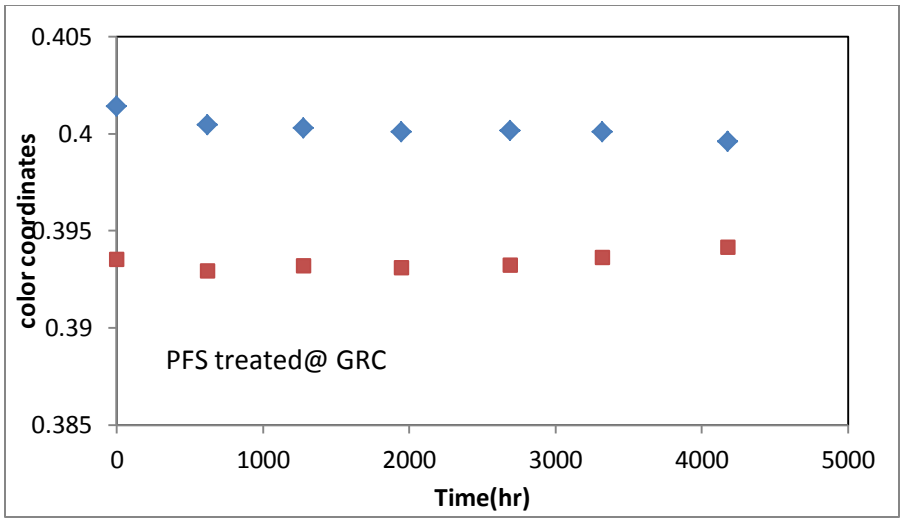

Figure 33. Shift in x and y color coordinates for PFS-based blend in a Vio^{TM}-like prototype

3. Next steps towards commercialization

Phosphor scale-up

As part of the deliverables of this program, we have demonstrated 50g synthesis methods to make phosphors with high quantum efficiency and appropriate particle sizes. Our identified toll vendor in Oklahoma has already demonstrated the ability to make PFS at 50g scale with equivalent efficiency to our current 5-10 g scale syntheses. However, we believe additional work will be necessary to improve the synthesis yield of these phosphors (currently at 50-60% of theoretical) in order to bring further bring down the phosphor cost. This will be critical in remote phosphor systems where phosphor usage will be much higher. For our green phosphors, we received samples from our prospective toll vendors in Pennsylvania and these samples essentially match the performance of samples made at GE. Consequently, we currently believe that there is minimal risk in the scale-up and synthesis of the phosphors developed in this program.

LED system design

Within this program, we have determined many of the benefits and limitations of our GE phosphor systems. Provided low incident fluxes and phosphor temperatures, we believe that these phosphors are significantly better than any commercial system currently available for high CRIs (Table 21). These systems are also competitive with hybrid LED systems that use red LEDs with the potential advantage of much simpler driver electronics. However, the limitations must be taken into account for any future LED system design. We briefly discuss these issues here.

The largest risk that exists before implementing these phosphors into lighting products is the reliability of these phosphors in representative light engines, especially the PFS phosphor. At the current time, there are both temperature and blue light flux limits for the use of this material. This could limit the use of PFS to only diffuse lighting systems where blue light fluxes and temperatures are low, somewhat limiting market penetration of LED systems that use this phosphor. Consequently, apart from prototyping of systems that can use PFS currently, we will be working towards further improving the flux and thermal stability of these Mn^{4+} line-emitting

phosphors through internal GE programs. This can involve both process and compositional modifications.

Even without any reliability concerns, there can be significant thermal losses in our light engines, especially when they are driven at currents higher than the nominal drive current. If the heating of the phosphor/silicone dome leads to additional heating of the LEDs (Figure 14), as surmised, then improved thermal management at the LED board should reduce these losses. In addition, there are additional green phosphor composition modifications to reduce quenching to ~5% at 125^{o}C, which should improve the steady-state performance of these parts. Furthermore, our modified synthesis samples with higher quantum efficiencies & reduced parasitic absorptions should also reduce somewhat losses and heating in the phosphor/silicone dome. However, we believe that there are intrinsic thermal issues in our light engines in that the phosphor/silicone dome is thermally isolated from all thermal management paths that are used to cool the LEDs on the circuit board (Figures 24 and 27). Consequently, it could be necessary to investigate alternate geometries and methods to improve cooling of the phosphor dome as well as create thermal paths from the phosphor/silicone dome to LED thermal management.

4. Milestones/Deliverables

This section is the same as the one given in the Executive Summary section earlier in this report.

Task 2:

Intermediate milestones

Title: Determine composition (i.e. activator concentration) vs. thermal quenching parameters & guidelines for concentration-based thermal quenching (6/15/2010)

Status: Characterized relative quantum efficiency from 25-200^{o}C for blue, green, orange, and red phosphors completed & developed fundamental model for high temperature quenching mechanisms.

Title: Measurements for optical constants (absorption coefficient, refractive index, scattering parameters) for current phosphor compositions (6/30/2010).

Status: Developed and verified methods to decouple absorption and scattering within powder phosphor. We are using measurement techniques to evaluate all phosphors in program. Also, determined that parasitic absorption is present in red-line emitting phosphors that need to be reduced/removed in order to optimize package efficiency.

Title: Initial optical model for remote phosphor packages & correlation with current GELS package performance under pulsed operation (8/15/2010)

Status: Developed two-flux model incorporating optical losses, scattering, phosphor quantum efficiency, and geometry of current Lumination packages that can predict package efficacy differences for both blue and violet LED packages. Used model to assign relative weights for package and phosphor modifications.

Title: Integrated optical & thermal models for remote phosphor package (9/15/2010)

Status: Developed fundamental understanding of thermal quenching in some of Ce^{3+}-phosphors (SASOF/YAG), need to integrate further into package models for steady-state performance. Developed methods to measure phosphor temperature *in situ* using the spectral parameters of the PFS red-line emitting phosphor.

Task 2 deliverable

Title: Design parameters for phosphor particle size and morphology combined with package design for 20% improvement in steady-state efficacy (9/30/2010)

Status: Package model has determined that 15-20% improvements are possible by increasing package reflectivity to ~90% with an additional 5-10% improvements are possible through reduction of phosphor scattering losses (@90% package reflectivity). Improvements from phosphor scattering will become larger at lower package reflectivities. Also, removal of parasitic absorption in the red line emitter can also lead to >5% improvement in package efficiency.

Task 3:

Intermediate Milestones

Title: Demonstrate larger particle size blue phosphor with semi-infinite plaque absorption >75% (vs. ~55% currently) with no loss in QE (RT & 150C) & similar plaque reliability (8/31/2010)

Status: Increased particle size and Eu^{2+} concentration in blue phosphor without concentration quenching. Modified phosphor stoichiometry and excess halide levels (fluxing) to improve reliability in plaque testing. Materials sent to GELS for lamp testing. Further work stopped due to focus on blue LED-based systems.

Title: Develop synthesis and/or coating methods to protect current green & deep red phosphors from 85C/85%RH (HTHH) conditions; <5% loss after 100 hrs under direct HTHH exposure (10/15/2010)

Status: Developed numerous coating strategies for SASOF green phosphor that minimize moisture sensitivity. No losses in phosphor quantum efficiency; optimization gives thinner coatings that minimize scattering losses. Materials sent to GELS for lamp testing.

Title: Demonstrate classification method to remove fine particles for current green and orange phosphor particles; improve semi-infinite plaque absorption by >5% versus non-classified particles

Planned Date: 11/30/2010

Status: Developed elutriation methods to remove fine particles from powder phosphors. Reduced phosphor scattering coefficients by >40%, yielding increases in d_{10} particle size and semi-infinite plaque absorption of 7-10% depending upon phosphor composition. Adopted as best practice for all phosphors in this program.

Title: Demonstrate synthesis method to increase particle size in current orange phosphor particles to increase semi-infinite plaque absorption by 10%

Planned Date: 3/31/2011

Status: Developed fluxing system for orange phosphor to increase particle size and semi-infinite plaque absorption at lower activator concentrations. Current issue with fluxing system is reactivity with furnace components reducing component lifetime. Using initial knowledge to modify furnace or fluxing system. Work stopped to focus upon synthesis of red-line emitting phosphor in order to simultaneously improve CRI & lumen equivalent.

Title: Demonstrate synthesis method to narrow particle size distribution in current green phosphor particles to d10~>8 μm
Planned Date: 3/31/2011
Status: Initial testing within our silicate garnet phosphors has shown that modification of the initial stoichiometry of the materials leads to a lower d_{10} of ~8 μm and a significantly larger plaque absorption. Optical testing of modified garnets whose fine particles were removed by decanting/elutriation showed improve phosphor conversion efficiency by ~3-5%.

Title: Optimize synthesis method for larger particle size green/orange phosphor to match current RT QE (6/30/2011)
Status: For the silicate garnet phosphors, our optimized synthesis method was based upon non-stoichiometric starting compositions to minimize 2nd phase formation and Ce^{3+} segregation into these 2nd phases. For our red-line emitting phosphors, we optimized the phosphor synthesis through control over precipitation processes.

Title: Iterative optimization of particle size/composition based upon model in Task 2 & Task 4 results (9/30/2011)
Status: We have continued phosphor optimization to minimize parasitic absorptions in these phosphors, primarily through removal of parasitic 2nd phases. The primary focus has been on our red-line emitting phosphor and control over the pH during synthesis to minimize K_2MnF_6 decomposition that both reduces the amount of Mn^{4+} incorporated into the phosphor and also leads to a brown parasitic absorption.

Task 3 final deliverable:
Title: Demonstrate synthesis at 50-100 g batch scale for optimized composition & synthesis with QE>85% and meeting size distribution and morphology requirements defined from Task 2 (12/30/2011)
Status: We have demonstrated 50 g scale-up of all green phosphors including the moisture protective coating of the SASOF phosphor. We have worked with a toll vendor in Pennsylvania (outside of this program) and have made these phosphors at larger scales. In addition, we have transitioned the synthesis of our red line-emitting phosphor to an external toll vendor in Oklahoma, and our external toll vendor has matched the quantum efficiency of our internal 5-10 g samples at 50 g scale.

Task 4:
Title: Demonstrate 10% steady-state package efficiency improvement (currently 65% at steady state) improvement versus current 350 lumen prototypes (12/15/2010)
Status: Demonstrated lumen improvement in lower lumen packages using reflective insets instead of typical printed circuit boards. Package efficiency is currently at 70% versus 65% in prior systems. Assigned one loss to parasitic phosphor absorption in red-line emitter phosphor.

Title: Demonstrate 10% steady-state package efficiency (currently 65% at steady state) improvement versus current 700 lumen prototypes (3/30/2011)
Title: Demonstrate 20% steady-state package efficiency improvement versus current 350 lumen prototypes (9/30/2011)

Title: Demonstrate 20% steady-state package efficiency improvement versus current 700 lumen prototypes meeting reliability (<1% lumen loss and d(u,v) shift of 0.003 over 5000 hrs of room temperature operation) (3/30/2012)
Status: We have tested the efficacy of various phosphor geometries using a light engines using a board populated with 7 Cree royal blue LED packages. We have generally found that hemispherical phosphor domes have significant improvements in efficacy versus cylindrical light engines in accordance with our optical models. Consequently, we are able to reach efficiencies of 78-82% in flash measurements & 72-76% phosphor efficiencies in steady state measurements at 350 mA drive currents. We have taken these values higher in linear light engines with angled side walls that have total efficiencies of ~85% with a phosphor/package efficiency of ~220 lm/W_{blue}. All of these values represent an improvement of >20% of our initial phosphor efficiency at the program start. In our current phosphors, we have found that there are both efficacy and reliability limitations when the steady-state phosphor temperature exceeds 80°C. Most of the reliability concerns come from the PFS red-line emitting phosphor, so we have also studied the reliability of this phosphor in greater detail. We also tested our phosphors for blue light damage under accelerated conditions using a blue laser. Taking the results from the accelerated damage experiments, we believe that our remote phosphor light engines should meet both lumen loss and color shift metrics for reliability, provided that the incident flux on the phosphor is <0.5 W/cm^2 with a phosphor temperature <80°C. We have initially validated these parameters through testing of PFS-based blends in Vio™-like prototypes and will be continuing reliability testing in various light engine configurations.

5. Program management

Filed patents
Layered phosphor-LED embodiments for white light emission
Ca rich garnet phosphor materials having enhanced spectral characteristics
Coating moisture-sensitive LED phosphors
Two disclosures under review for prior art

Issued patents & published applications (including prior DOE programs)
"Color-stable manganese phosphors," US8252613 (2012).
"Alkaline and alkaline earth metal phosphate halides and phosphors," US20120049116 (2012).
"Coated phosphors, methods of making them, and articles comprising the same," US20110147664 (2011).
"Color stable phosphors," US20110279011 (2011).
"Alkaline earth borate phosphors," US20110127905 (2011).
"Kimzeyite garnet phosphors," US20110089817 (2011).
"Blue-green and green phosphors for lighting applications," US20100096974 (2010).
"Green emitting phosphors and blends thereof," US7857994 (2010).

Conference presentations
Quenching of orange-red Ce^{3+} luminescence in garnet hosts," 2010 DPC, Argonne.
"Site occupancy, charge compensation, and quenching in $Sr_3AlO_4F:Ce^{3+}$-based phosphors," 2010 Fall ECS, Las Vegas.

"Synthesis and luminescence properties of green oxynitride phosphor," 2010 Fall ECS, Las Vegas
"Phosphors for blue and violet LED systems," 2011 Phosphor Global Summit, San Antonio.
"Concentration Quenching in Ce^{3+}-based LED Phosphors," 2011 International Conf. on Luminescence, Ann Arbor.
"Solution-based Protective Coatings for LED Phosphors," 2011 Fall ECS, Boston.
"Luminescence Quenching in Highly Doped YAG:Ce," 2011 Fall ECS, Boston.
"Sensitizing Eu^{3+} for potential LED phosphors," 2011 Fall ECS, Boston.
"Phosphors for blue & violet LED systems," 2012 Photonics West, San Francisco.

Journal articles & conference proceedings
"Sensitizing Eu^{3+} with Ce^{3+} and Tb^{3+} to make narrow-line red phosphors for light emitting diodes," Electrochemical and Solid-State Letters **15**, J25 (2012).
"Concentration quenching in Ce^{3+}-doped LED phosphors," J. Lumin., accepted.
"High efficacy and color rendering light-emitting diode lamps using oxyfluoride and fluoride phosphors," Chem. Mater., **22**, 4076 (2010).
Three additional articles under preparation